PERFORMANCE ANALYSIS OF A QUASI-SYNCHRONOUS DS-CDMA WIRELESS LOCAL LOOP SYSTEM

by

Richard Wai Shing Lee

A thesis submitted in conformity with the requirements
for the degree of Master of Applied Science,
Graduate Department of Electrical and Computer Engineering, in the
University of Toronto, Canada

395 Wellington Street
Ottawa ON K1A 0N4
Canada

395, rue Wellington
Ottawa ON K1A 0N4
Canada

Your file Votre référence

Our file Notre référence

0-612-29412-9

Canada

Abstract

PERFORMANCE ANALYSIS OF A QUASI-SYNCHRONOUS DS-CDMA WIRELESS LOCAL LOOP SYSTEM

by Richard Wai Shing Lee.

Master of Applied Science, 1997.

Department of Electrical and Computer Engineering, University of Toronto.

In this thesis, a quasi-synchronous reverse link system is proposed as an alternative to the existing DS-CDMA system, such as the IS-95, to provide the wireless local loop services. The goal of quasi-synchronizing the reverse link transmissions is to reduce multiple access interference, which is a major factor that limits the system capacity of a CDMA system.

In the thesis, a synchronization scheme is proposed to achieve the 1/2 chip synchronization in the reverse link of a wireless local loop system. Analytical expression for the reverse link synchronization time is derived. Comparison of the performance for a coherent synchronization system and a non-coherent system is given. Recommendations are presented to reduce the effect of multiple access interference on the synchronization time. In the second part of the thesis, high spectral efficiency modulation schemes are found to increase the barrier that limits the cell capacity for systems using orthogonal spreading codes. The performance in terms of frame error rate for different modulation and coding schemes is obtained through simulation. Finally, the use of receiver antenna diversity and directional transmitter antennas to increase coverage and reduce multiple access interference is also presented. Simulation results are obtained to analyze the overall capacity for the reverse link of a wireless local loop system in various situations.

Acknowledgements

I would like to express my gratitude to Professor E. S. Sousa for his supervision and valuable advice throughout the course of this research work. I would also like to thank Jonathan Sau, Michael Yu, Wilson Wong, Edward Mah, Chris Gao, Leycheoh Lim, and many others from the wireless group for their suggestions and comments.

I am indebted to my parents for their support and continued encouragement during the course of my study.

Finally the financial support through a fellowship by Information Technology Research Centre (ITRC) is gratefully acknowledged.

Richard Wai Shing Lee
April, 1997

Contents

List of Tables

List of Figures

Chapter 1

Introduction

In the past few years, the liberalization of telecommunications services in many countries has caused high competition among telephone companies with the challenges of providing basic telephone services, enlarging existing capacity and managing infrastructure in a speedy and cost-efficient way. Radio becomes ideal for use in the local loop. The generic term used to describe telephone systems where the final link to a fixed location is made using radio is known as radio in the local loop (RLL) or wireless local loop (WLL). The use of radio instead of copper wire to connect telephone subscribers has a number of advantages: it provides quick deployment of telephone services to developing countries where the need for telecommunications far exceeds the ability to install wireline infrastructure in a timely manner, it has a low initial installation cost, its maintenance costs are also far lower than the costs for wired networks. Finally, the radio infrastructure can easily be dismantled and re-installed in another area.

As shown previously radio not only provides a convenient medium for mobile communications, it also has many advantages in providing fixed network access. Currently due to the cost consideration of redesigning a WLL system, many operators and manufacturers are using the existing mobile cellular equipment to provide the local loop services. As will be demonstrated later, because of the difference in service requirements and channel characteristics, the mobile cellular architecture should be modified to gain more capacity for use in fixed wireless systems.

The following sections give a brief description for different multiple access schemes,

using different techniques in DS-CDMA WLL systems, such as synchronous reverse link transmission and different coding and modulation schemes.

1.1 Multiple Access Schemes

In today's digital cellular systems, numerous users transmit to and receive from the same base station simultaneously through three major types of multiple-access techniques namely, frequency division multiple access (FDMA), time division multiple access (TDMA), and code division multiple access (CDMA). In FDMA, the frequency spectrum is divided into segments and assigned to different users. Thus, users' signals are orthogonal in frequency. In TDMA, each user transmits for a fraction of time over the whole spectrum. Since users' signals are transmitted at different time, they are orthogonal in time. Finally, in the CDMA technique users' digital signals are spread over the entire frequency spectrum with different spreading codes that, ideally, should have very low correlation among each other. At the base station, different users' signals are then recovered by correlating the received signals with the assigned spreading codes. The process is known as despreading.

Ideally, in a single cell system, the performance of the three multiple-access techniques is the same for systems using the same modulation scheme [1]. That is the number of users that can be accommodated is equal to the total available spectrum, W, divided by the required date rate, R, assuming that all systems use BPSK modulation and Nyquist pulse shape with no excess bandwidth. However, this ideal performance can never be achieved in practice due to interference caused by the adjacent channels in both FDMA and TDMA system. Therefore, guard bands and guard times are always required to minimize the adjacent channel interference. For CDMA the non-perfect synchronization of transmissions among users and the existence of multipath cause high interference to all users, called multiple access interference (MAI).

In a multiple cell environment, a fair comparison for the performance of the three different multiple-access schemes becomes very difficult. And the result depends on the availability of technologies, the environment of operations, and the assumptions

[1] It is assumed that the CDMA system employs orthogonal spreading codes.

made. However, CDMA does offer some advantages that cannot be found in FDMA and TDMA [1], [2]. The two major issues that cause degradation in system capacity in a terrestrial mobile wireless network are the multi-user interference and the multipath propagation [3]. The first problem is solved in the CDMA system by spreading each user's signal such that the multi-user interference can be modelled by Additive White Gaussian Noise (AWGN) which is the interference that communications engineers are familiar with (e.g. coding and modulation performance are well known for AWGN channel). In an environment with multipath propagation, different replicas of the signal arrive with different delays. For TDMA and FDMA systems with narrow-band signals, these replicas cannot be resolved and they are combined constructively or destructively causing fading. For a CDMA system the replicas of the wide band spread spectrum signal with different delays that are greater than one chip period can be resolved and combined constructively using a RAKE receiver [4]. Another economic benefit of CDMA is its potential to provide higher cell capacity over FDMA or TDMA. This is due to its feature of universal frequency reuse. Thus, in CDMA, the entire frequency band is shared by every user in all cells, which not only relieves the need for frequency planning, it also increases the cell capacity. Due to these superior features, CDMA has been adopted as the second North American digital cellular standard, called the IS-95 [5].

1.2 DS-CDMA Systems for Mobile Communications

1.2.1 Transceiver Model

A typical structure of a DS-CDMA transmitter/receiver pair is shown in Figure 1.1. At the transmitter, the user's data stream $d(t)$ is first spread by a unique spreading sequence $c(t)$ to occupy a much wider bandwidth. The signal is then modulated to a carrier at frequency ω_c. If we denote the bandwidth of the spreading code to be $W = 1/T_c$ and the data rate to be $R = 1/T_b$, the processing gain, which is defined as

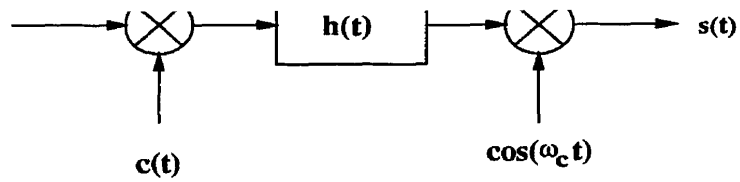

DS/CDMA Transmitter

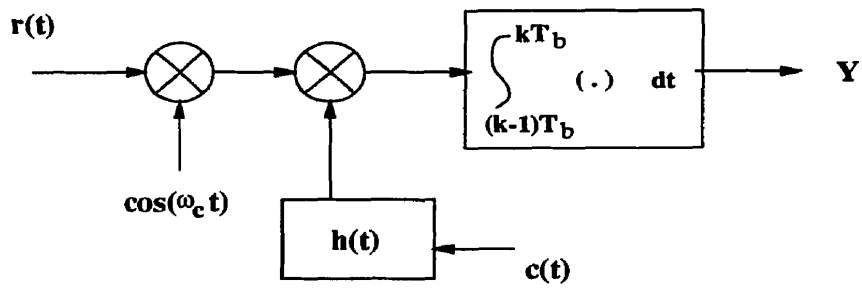

DS/CDMA Receiver

Figure 1.1: Block diagram for a DS/CDMA transceiver

the bandwidth expansion, is expressed as

$$M = \frac{W}{R} = \frac{T_b}{T_c}, \tag{1.1}$$

where T_b is the bit symbol interval and T_c is the chip interval.
The transmitted signal is then given by

$$s(t) = \sqrt{E} \sum_{i=-\infty}^{\infty} d_{\lfloor i/M \rfloor} c_i h(t - iT_c) \cos(w_c t), \tag{1.2}$$

where $\sqrt{E}$, d_i, c_i are the signal amplitude, data sequence, and chip sequence, respectively. M is the processing gain given in (1.1) and $h(t)$ is the chip pulse shape. $\lfloor x \rfloor$ denotes the largest integer smaller than or equal to x.

At the receiver front end, the received signal $r(t)$ is expressed as

$$r(t) = \sum_{k=1}^{N_u} \sum_{l=1}^{L} \alpha_{k,l} s_k(t - \tau_{k,l}) + n(t), \tag{1.3}$$

where N_u, L, α, τ, θ are the number of users, number of paths, fading amplitude, time delay, and carrier phase, respectively. $n(t)$ is a background noise process with power spectral density $N_o/2$. Other symbols are defined in (1.2). This received signal is then demodulated and despread by the corresponding user's spreading code. The decision variable is obtained by integrating and sampling the demodulated signal with period T_b and is given as

$$y = \pm M\alpha\sqrt{E} + \psi + \eta. \tag{1.4}$$

The first term is the desired signal, second term is the multiple-access interference, and the last term is an AWGN sample.

The statistics of the fading amplitude and the multiple-access interference are the two most important factors in determing the performance of a CDMA system. A brief review of these topics is given in the below sections.

1.2.2 Multiple Access Interference

Multiple access refers to the simultaneous transmissions by numerous users to a common receiving point. In a CDMA system, all users share the whole spectrum in all cells. Therefore, a spreading sequence having noise-like auto-correlation[2] and uniformly low cross-correlations with any other spreading sequences is assigned to each user. A commonly used pseudo-noise (PN) sequence is generated by a set of linear feedback shift registers (LFSR) which has a maximum period of $2^n - 1$, where n is the number of stages of the feedback shift registers [6]. In IS-95, the long code and short code are generated by a LFSR with maximum period called m-sequence; the long code has a period of $2^{42} - 1$ and the period of the short code is equal to 2^{15}.

The noise-like correlation property of m-sequences is realized only when full period correlation (FPC) is employed at the receiver. Full period correlation is impractical when the PN sequence used has a long period such as those used in IS-95. This is because long acquisition time in most communications systems is intolerable. Also to support a given data rate in the available spectrum, the correlation period is usually limited (e.g. the correlation period is 64 chips per coded bit for IS-95). In this case, most receivers use partial period correlation (PPC). In a system that adopts partial

[2]the auto-correlation function for additive white noise is a delta function

segments are masked onto the coded bit before transmission.

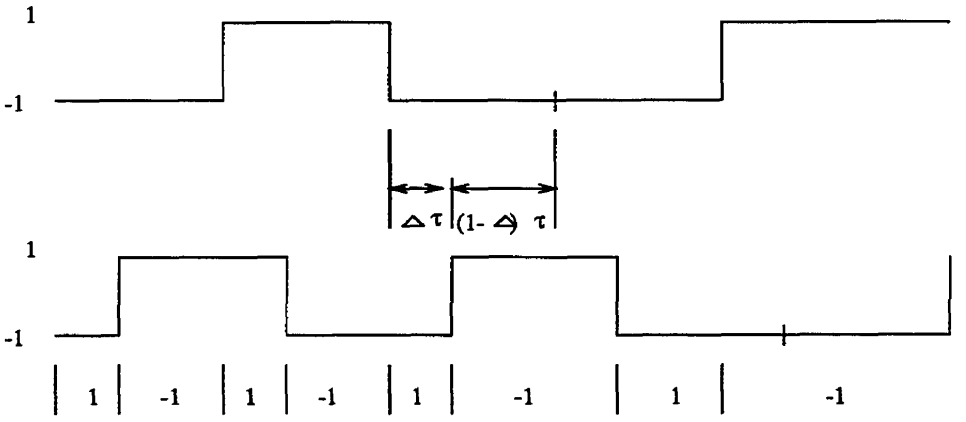

Figure 1.2: Partial sequence correlation

Analyzing the partial correlation property of PN sequences involves finding the correlation for all PN sequences with different code phase offsets. Even for PN sequences with moderate length, it becomes an intractable task. One approach is to find a set of sequences in which each sequence has good randomness properties. When the period of the spreading code is much longer than the observation period, the small segment of the m-sequences can be approximated by a random sequence [6]. Figure 1.2 describes the partial sequence correlation for a sequence of rectangular chip pulses. If we assume the use of rectangular chip pulse and for an observation period of M chips, we can express the correlation function as a summation of two random variables (rv's) $r_1 = \Delta c_i^1 c_{i+D}^2$ and $r_2 = (1-\Delta) c_i^1 c_{i+D}^2$, where c^1 and c^2 are indepedent random sequence with c_i^1 and c_{i+D}^2 equal to 1 or -1 and D is the chip offset between the sequences. r_1 and r_2 then take on value $\pm\Delta$ and $\pm(1-\Delta)$, respectively. We denote E_c be the chip energy for the rectangular pulse and T_c be the chip period. Then the correlation between two spreading codes for $D > 1$ [3] is given as

$$R = \sum_{i=1}^{M} E_c(r_1 + r_2). \tag{1.5}$$

For $M \gg 1$, we apply Central Limit Theorem and the correlation, R, becomes Gaus-

[3] in practice different users in a CDMA cellular system are assigned the same PN sequence with different offsets and $D \gg 1$

$$\sigma^2 = E_c(1 - 2\Delta + 2\Delta^2)M. \tag{1.6}$$

Multiple access interference (MAI) is then a result of the non-zero cross-correlation among spreading codes.

The above analysis of MAI assumes the use of random spreading sequence. It has been shown that after despreading, the interference power is approximately reduced by the processing gain [7]. The multiple access interference increases as the number of users in the system increases. This accounts for the lower cell capacity for using CDMA in a single cell system as compared to TDMA and FDMA. We can improve the capacity of a CDMA system by assigning orthogonal spreading codes to the users in the same cell. This is done in the forward link (the transmissions from the base station to the mobiles) of IS-95. In a point to multipoint transmission, the base station is able to coordinate all the transmissions of the orthogonal signals. As a result, interference only arises from other cells (inter-cell interference). However, for a systems operating in a multipath environment, interference caused by users of the same cell (intra-cell interference) and interference coming from the delayed version of the desired signal (inter-path interference) still exist and cause performance degradation to CDMA systems.

In the reverse link (transmissions from mobiles to the base station), the coordination of users' transmission becomes impossible as rapid movement of users causes problem in maintaining synchronization. As a result, users are usually assigned long period PN spreading codes instead.

1.2.3 Multipath Fading Channel

The complex low-pass equivalent impulse response of the multipath channel for the k^{th} user is written as [8]

$$h_k(t) = \sum_{l=1}^{L} \alpha_{k,l}\delta(t - \tau_{k,l})e^{-j\theta_{k,l}}, \tag{1.7}$$

where $\alpha_{k,l}$, $\tau_{k,l}$, and $\theta_{k,l}$ are the signal amplitude received from the l^{th} path, the time delay of the l^{th} path relative to the first path and the random phase shift, respectively. The average number of resolvable paths, L, is then given by

$$L = \lfloor \frac{T_D}{T_c} \rfloor + 1, \tag{1.8}$$

where T_D is the RMS delay spread, T_c is the chip duration, and the function $\lfloor x \rfloor$ equals the largest integer smaller than or equal to x. Since the receiver cannot resolve paths that arrive with relative delays less than T_c, the signal amplitude $\alpha_{k,l}$ consists of paths that are combined constructively or destructively. The amplitude variation due to the multipath characteristics of the channel is named channel fading. In dense urban environments, the fading amplitudes $\alpha_{k,l}$ for $l = 1, 2, \cdots, L$ are usually modelled as identically distributed independent Rayleigh random variables, because in such environment, there exists a large number of reflections and the transmitter-receiver pair is rarely visibile [9, 10].

In a multipath fading environment, fading amplitudes are correlated in both time and in frequency. The degree of correlation depends on the coherence bandwidth Δf_c and coherence time Δt_c of the channel. The coherence bandwidth of the channel is measured as the inverse of the delay spread, i.e, $\Delta f_c \approx \frac{1}{T_D}$. The fading amplitude of two sinusoidal signals with frequency separation larger than Δf_c will have correlation less than 0.5. When the coherence bandwidth is small in comparison with the bandwidth of the transmitted signal, the channel is said to be frequency-selective; otherwise, the channel is said to be frequency-non-selective or flat fading channel [11].

The coherence time, Δt_c, is inversely proportional to the Doppler spread

$$B_d = \frac{v}{c} f_c, \tag{1.9}$$

where v is the velocity of the mobile unit, c is the speed of light, and f_c is the carrier frequency. The signals received with time separation longer than Δt_c are assumed to experience independent fading.

As mentioned in the above section, multipath fading causes large variation in the received signal strength. In order to guarantee a satisfactory quality of service at most times, the system always operates in a higher signal to interference plus noise ratio (SINR) than the minimum required SINR. The difference between the minimum required transmit power and the actual operating power in the fading environment is known as the fading margin.

Power control is used in CDMA to alleviate the above problem. By controlling the signal powers to be the lowest necessary, we minimize the total level of interference such that more users can be served with acceptable quality. In addition, power control is also essential to combat the near-far problem in which the received power from users near the base station causes undue level of interference to far-out users.

In IS-95, power control is done at the reverse link in two levels [5], open-loop power control and closed-loop power control. In the open-loop power control scheme, the mobile adjusts its power according to the received power of the pilot signal; for example, a higher power is transmitted whenever the received power is lower. This open-loop power control scheme can only compensate for the propagation attenuation and the channel shadow fading effect. The rapid signal variation caused by the Rayleigh fading is then compensated by the closed-loop power control scheme. In IS-95, the base station measures the received signal strength and transmits power control information to the mobiles at 800 bps. The mobiles then adjust their transmit power 800 times per second with .5 dB per step.

1.2.5 Sectorization

Sectorization is a very effective technique to reduce multiple-access interference and is widely used in the terrestrial mobile wireless networks to increase cell capacity. Theoretically, a CDMA system with n sectors per cell has a cell capacity n times better than the non-sectorized system. However, the improvement in cell capacity is always less than n in practice because a receiver antenna with infinite attenuation outside the main lobe is impractical to build. So, signals received from other sectors still interfere with the desired user's signal, but in much smaller magnitude.

there are other issues that limit the sector size; for example, the rate of hand-off, which happens when the mobile users move to the adjacent sectors, is high for cells with small sectors. This results in a lot of signaling between sectors and, thus, causes inefficient utilization of the system bandwidth. The two commonly used sector sizes in today's cellular networks are 3 and 6 sectors per cell.

1.3 Overview of DS-CDMA Wireless Local Loop Systems

Figure 1.3 shows a diagram of a typical cell structure for a WLL system. The cell structure is similar to that used in mobile communications. The transceiver model described in Section 1.2.1 and the analysis of multiple-access interference for DS-CDMA mobile systems in Section 1.2.2 apply to the wireless local loop system as well. The main differences that distinguish a wireless local loop system from the conventional cellular systems are the environment of operations, antenna height at the subscriber terminals, and the stationarity of users. Because of these differences, the channel characteristics for a local loop system are generally much different.

Since the antenna in the subscriber terminals can be mounted on the roof of buildings, it is generally located in a higher position than the mobile antenna. As a result, a direct propagation path usually exists between the base station and the subscriber terminals. The situation in which there exists a strong signal in a communication channel is called line of sight (LOS) communication. In the case where LOS is available, the multipath fading amplitudes become Rician random variables, and the variation of signal strength is much smaller than the variation of amplitude with Rayleigh distribution, commonly seen in the mobile environment. In addition, because the users are stationary, the communication channel is relatively time invariant. The disadvantage of a static channel is that time diversity scheme cannot be applied in such a channel. On the other hand, power control becomes very effective in a static channel. Thus, less over-head is required to send power control information and high capacity can be realized with less power control error. Finally, the wireless

wire is not economical. It is found that the RMS delay spread for sub-urban area is roughly equal 500 ns [10]. For system bandwidth of 1.25 MHz specified in IS-95, there exists only one resolvable path.

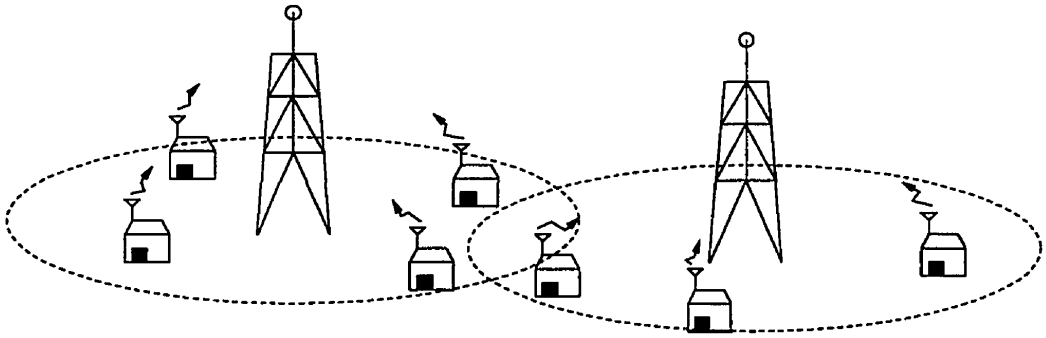

Figure 1.3: Cellular structure for a WLL system

1.4 Thesis Objective

As mentioned at the beginning of the this chapter, there is no current standard for DS-CDMA wireless local loop systems. Operators use the available mobile cellular standard such as IS-95 and apply it to provide the local loop services. The motivation for this thesis is to exploit the potential of using more sophisticated techniques to achieve higher capacity for the wireless local loop system.

The two most important factors that cause performance degradation in a DS-CDMA system are known to be the effect of multipath fading and the multiple-access interference. The effect of multipath fading in a WLL system is not so severe and with power control multipath fading can easily be compensated. As a result, we will focus on techniques that are efficient in combating multiple-access interference. The use of orthogonal spreading codes with synchronous transmission has been shown to be very effective in alleviating the effect of intra-cell interference [12] and it has been adopted in the forward link of IS-95. For a WLL system, since the channel is static, synchronization in the reverse link can be achieved with small increase in system complexity. Thus, it is interesting to find a synchronization scheme, analyze its performance, and compare the synchronous reverse link system with the IS-95

schemes should be found to maximize the number of orthogonal users in the system.

To further increase cell capacity, we have to reduce also the inter-cell interference. Although sectorization is already used to achieve higher capacity, the sector size is limited in order to have high trunking efficiency. Directional transmitter antennas can then become very useful for combating inter-cell interference. The use of a directional transmitter antenna is suitable for the local loop system because the location of both the base station and the subscriber terminals is fixed.

1.5 Thesis Organization

The thesis is organized as follows:
In Chapter 2, we examine the advantage of quasi-synchronizing the reverse link transmissions to within 1/2 chip period. We then show a simple scheme to achieve the synchronization. The reverse link synchronization time is analytically derived and the performance of a coherent synchronization system is compared with a non-coherent system. Effect of multiple access interference on system performance is studied and recommendations are given to relieve the problem.

In Chapter 3, we look at some possible coding schemes that can be used for systems with quasi-synchronous reverse link. Also, a higher spectral efficiency QPSK modulation scheme is proposed to increase the number of orthogonal users and still preserve the orthogonality of spreading codes. Advantages and disadvantages of this modulation scheme as compared to the modulation used in IS-95 are examined. Simulation results are obtained to determine the required SINR for achieving acceptable speech quality using the proposed coding and modulation schemes. Simulation is also done for 16-QAM and 8 PSK Trellis coded modulation for comparison.

In Chapter 4, we simulate the overall system performance of a quasi-synchronous DS-CDMA WLL system. Other factors like shadow effect, intra-cell, and inter-cell interference are also considered. We also study the advantages of using directional antenna and sectorization. Finally, an overall comparison between the synchronous and asynchronous WLL system is presented.

Chapter 2

Synchronization System for the Reverse Link of DS-CDMA WLL Systems

As mentioned in Section 1.2.2, multiple access interference (MAI) caused by non-zero cross-correlation between different spreading sequences is one of the major factors that limits the capacity of a CDMA system. In this chapter, we attempt to reduce the MAI by employing orthogonal spreading sequences and synchronizing the reverse link transmissions at the chip level (quasi-synchronization). In this thesis, whenever the word "synchronization" is used, it is meant to be the process of coordinating the user transmissions such that the different users signals are aligned when they arrive at the base station, and the word "quasi-synchronization" is used when the user signals are aligned to within a fraction of a chip time. Other synchronization schemes such as the PN code synchronization and carrier phase synchronization will be stated clearly if used in any context. Synchronization of the reverse link transmissions is generally difficult to achieve in a cellular system due to the variation of propagation delays and the difficulty of maintaining synchronization of the various mobile users. Since users in the WLL system are stationary, the propagation and transmission delays can be compensated for at the beginning of the calls. A coherent synchronization system for the reverse link of the wireless local loop system is designed for this purpose.

The chapter starts with a brief description of the synchronous reverse link channel

by an analysis of the reverse link synchronization time. The effect of MAI during the synchronization process and recommendation for improvement are also given. Finally, the performance of a DS-CDMA system with quasi-synchronous reverse link is analyzed, and the advantages and trade-offs of a synchronous reverse link in the WLL system are summarized at the end of the chapter.

2.1 Synchronous Forward and Reverse Link Channel Model

The orthogonal spreading sequences used in this thesis is assumed to be the Sylvester sequences, also known as Walsh sequences. The $n = 2m$ order Walsh sequences are generated recursively as follow

$$H_{2m} = \begin{bmatrix} H_m & H_m \\ H_m & -H_m \end{bmatrix}, \tag{2.1}$$

where $H_m = 1$. In a system in which user transmissions are not perfectly synchronous, Sylvester sequences have been shown to yield the lowest average cross-correlation [12]. As in the other DS-CDMA systems, users from all the cells share the whole frequency spectrum. In addition, because the number of orthogonal sequences is limited [1], PN sequences are masked to the orthogonal sequences so that the set of orthogonal sequences can be reused in the other cells. Note that the same PN sequence is assigned to all users in the same cell to preserve the orthogonality of the spreading sequences.

The forward link of our system, like IS-95, is assumed to consist of two broadcasting channels, namely the pilot channel and the synchronization channel. The rest of the channels in the forward link are assigned for paging the user terminals (called the paging channels) and traffic carrying (called the traffic channels). Since we are interested in the reverse link synchronization, the only channels of interest in this chapter are the pilot channel and synchronization channel. Functions of the two channels are given later.

[1] the number of orthogonal sequences is determined by the system bandwidth and data rate.

channels (for accessing the network) and traffic channels (for traffic carrying from user terminals to the base station). The total number of channels in both links is then determined by the available number of orthogonal spreading codes. An example of a user terminal initialized reverse link communication is given below.

When the subscriber terminal powers up, it attempts to synchronize to the pilot channel which carries no information except an unmodulated PN spreading code with a short period for fast acquisition. Once the state of the pilot signal is acquired, the terminal loads this information into its local PN generator to generate its masking sequence and then uses it to gather, from the synchronization channel, information regarding the current status of the base station. The terminal then starts transmitting to the access channels. If free channels exist at the base station, the terminal is acknowledged through the paging channel and communication is established in the assigned traffic channel.

As shown in the above example, the user terminals are synchronized to a different delayed version of the pilot signal because of the difference in propagation delays between terminals. As a result, when the different users' signals, which are synchronized to delayed version of the pilot signal, arrive at the base station, they are not aligned to each other, and the code phase offset among these signals can be as large as a few tens of chips depending on the location of users. In the next section, we will look at the design of a system to achieve 1/2 chip synchronization in the reverse link.

2.2 Reverse Link Synchronization System

2.2.1 Synchronization Scheme

The proposed synchronization system is aimed to synchronize all user signals to within half a chip period. The reverse link synchronization procedure is as follows: the base station receivers first synchronize to the spreading code of the received signals. Then, the proposed base station synchronization system measures the timing difference between the received signal and the reference clock, and sends control bits back to the subscriber synchronization system for appropriate adjustment. Figure 2.1 shows an

example of timing offsets for the signal transmitted from the user terminal and the signal received at the base station. τ_u and τ_B are the timing offsets for terminal u and base station B, respectively. τ_p is the propagation delay and $\tau_{UB} = \tau_u + \tau_p - \tau_B$ is the relative offset between the signal at the base station receiver and the reference clock. In this case, τ_{UB} is sent to the terminal u to request a shift of its clock by $-\tau_{UB}$. After adjustment, the new offset becomes $\tau_{UB'} = (\tau_u - \tau_{UB}) + \tau_p - \tau_B = 0$. Since in this thesis we only synchronize user transmissions to within 1/2 chip period, τ_{UB} is expressed in unit of 1/2 chip; i.e $\tau_{UB} \in \{0, 0.5, 1, 1.5, 2, 2.5 \cdots, n_{max}\}$ where n_{max} is the maximum possible code phase offset determined by the maximum distance between the terminals and the base station. The above procedure is realized by a synchronization system which includes units on both the subscriber terminal and the base station. The master synchronization unit is located at the base station; it measures the offset of all received signals and sends out commands to the terminals for correct adjustment. The synchronization unit at the subscriber terminal is a slave which receives instruction from the base station unit and adjusts the transmitter clock accordingly. The structure of both units is given in the next two sections.

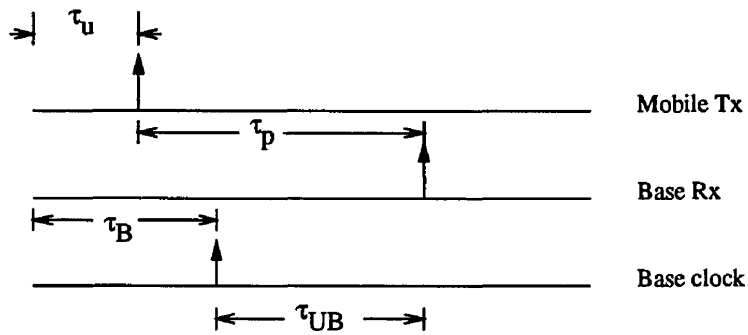

Figure 2.1: Timing offsets for signals transmitted from the user terminal and signals received at the base station

2.2.2 Subscriber Terminal Synchronization Unit

Overview of Operation

A block diagram for the structure of a subscriber terminal transmitter is shown in Figure 2.2. When the control unit receives the control bits, τ_{UB}, from the base station, it requests the state detection unit and the orthogonal sequence to advance

clock to skip half a chip cycle. The two phase clock is required to facilitate half chip adjustment because the PN generator can only advance by an integer number of states. Both the orthogonal sequence and the PN sequence are then masked onto the data signal before modulation to the carrier frequency. A detailed description of the 5 major components, a control unit, a 2-phase clock generator, a PN generator, a state detection unit, and an orthogonal sequence generator, is given below.

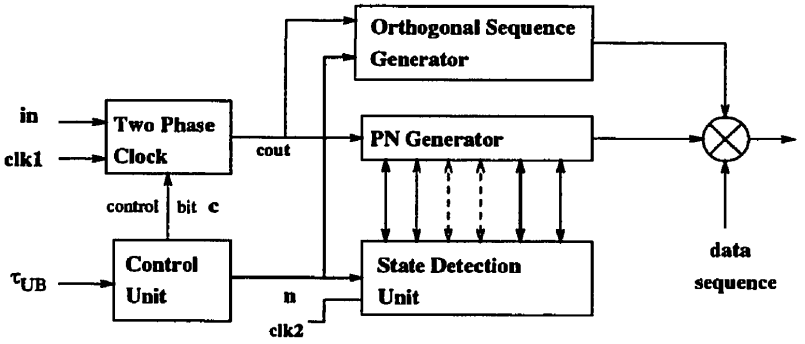

Figure 2.2: Block diagram for the transmitter of the subscriber terminal

Control Unit

The control unit is an intelligent unit which receives the control bits τ_{UB} from the base station. If $\lceil \tau_{UB} \rceil \neq \tau_{UB}$, the unit sets the output **n** to $\lceil \tau_{UB} \rceil$ and toggles the control bit **c**. Otherwise, it sets **n** to τ_{UB}. In addition, the unit only allows transition of control signal to occur at the positive rising edge of the clock signal, **cout**. In this way, the unit can only skip instead of adding chip cycle. For example, if the control command $\tau_{UB} = 3.5$, the control unit requests the state detection unit to advance the current state of the PN generator by 4. At the same time, it toggles the control signal such that the clock signal is skipped by 1/2 cycle. The net effect is that the state of the transmitted signal is advanced by 3.5 chips.

Two Phase Clock Generator

The two phase clock generator circuitry is shown in Figure 2.3. The flip-flop is driven by an external clock signal **clk1**, running at twice the chip rate which is equal to

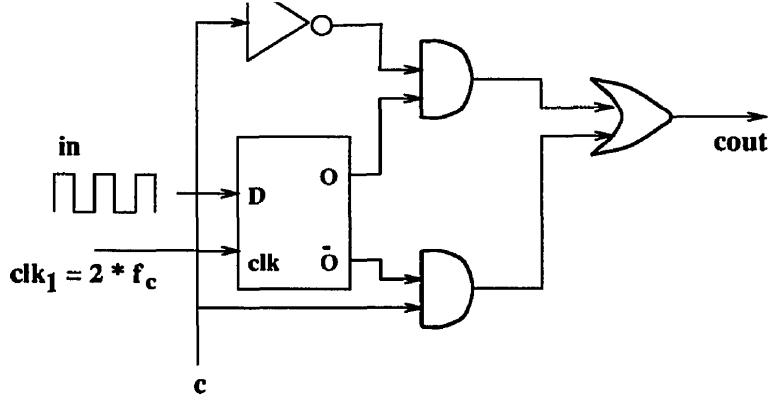

Figure 2.3: Two phase clock generator circuitry

1.2288 Mcps in our system. The input of the flip-flop **D** is another clock signal, **in**, that is phase locked to the pilot signal running at 1.2288 Mcps. From the timing diagram shown in Figure 2.4, we see that when the control signal **c** is "low", the output of the generator, **cout**, is taken from output **o** of the flip-flop; otherwise, when the control signal is "high", the output is taken from output $\bar{\mathbf{o}}$ of the flip-flop. As a result, whenever there is a toggle in the control signal **c**, the circuit skips half a chip cycle. The skipping of 1/2 chip cycle is necessary to delay the PN sequence and the orthogonal sequence by 1/2 chip period.

PN Generator

The PN generator consists of a linear feedback shift register (LFSR) for producing the pseudo-random sequence with maximum period, called m-sequence. One generator polynomial for creating the m-sequence with period $2^{15} - 1$ is $x^{15} + x^{13} + x^9 + x^8 + x^7 + x^5 + 1$. An example of the LFSR configuration for polynomial $x^3 + x + 1$ is shown in Figure 2.5. The PN sequences are used in the WLL system so that the orthogonal spreading sequences can be reused in the other cells. The partial period correlation property of the m-sequences is thoroughly reviewed in Section 1.2.2.

State Detection Unit

The state detection unit is another LFSR with the same configuration as the PN generator except that it is driven by a clock signal **clk2** having a frequency much

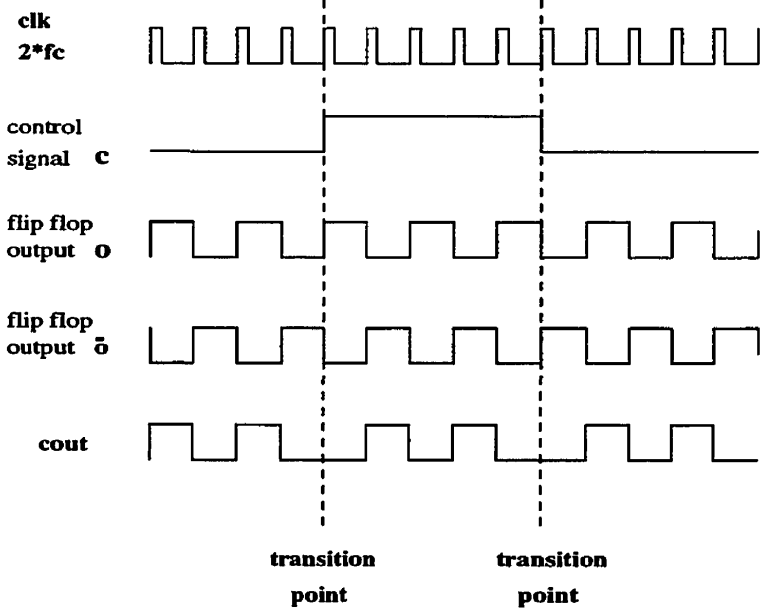

Figure 2.4: Timing diagram of clock generator circuitry

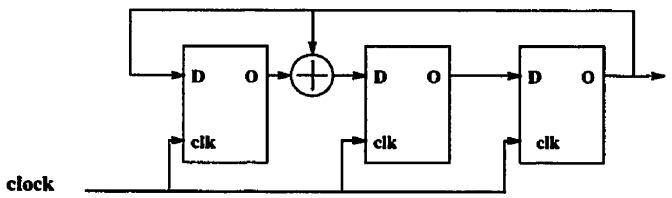

Figure 2.5: LFSR configuration with polynomial $x^3 + x + 1$

greater than the chip rate. The detection unit retrieves the current state of the local generator, advances the current state by a value specified by the input **n**, and loads the advanced state back to the PN generator.

Orthogonal Sequence Generator

Since the orthogonal sequence generator and the PN generator are driven by the same clock signal **cout**, both sequences are synchronized in code phase. The Sylvester sequences (also called Walsh sequences) are stored in a look up table. The sequence number which specifies the traffic channel to be used for reverse link communication is acquired from the base station at the beginning of the call. Walsh chips are then read out at chip rate (i.e. 1.2288 Mcps).

2.2.3 Base Station Synchronization Unit

The base station synchronization unit is a small modification of the PN code acquisition system. When the decision variable at the output of the correlator is greater than the threshold (initial PN code synchronization is achieved), the base synchronization unit measures the offset between the received signal and the reference clock. Control bits are then sent to the terminal to compensate for the offset. Figure 2.6 shows a block diagram for the base station synchronization system. The functions of the major components, such as the automatic threshold control and the base synchronization unit are presented below.

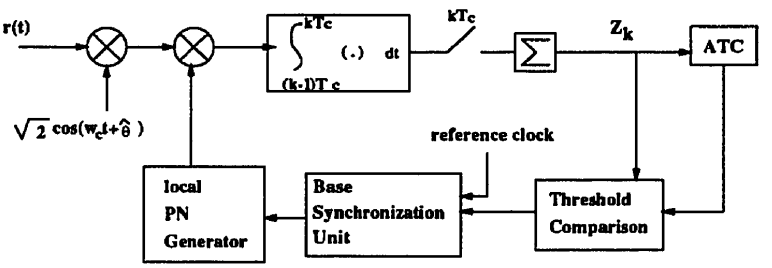

Figure 2.6: Base station synchronization system

Base Synchronization Unit

When PN code synchronization is achieved, the base synchronization unit compares the current state of the local PN generator with the state of the reference clock signal. The phase offset between the received signal and the reference signal is then transmitted back to the corresponding terminal. Since all receivers at the base station share the same reference signal, by synchronizing to this signal, the transmissions of all terminals are synchronized. In this thesis we are interested in 1/2 chip synchronization; thus, the phase offset, τ_{UB}, is expressed in unit of 1/2 chip period.

If we consider a cell size of a few kilometers and chip rate of 1.2288 Mcps, the propagation delay is less than 64 chip times. So, the base synchronization unit is required to set a timer to re-synchronize the local PN generator 64 chips after it sends out the synchronization command. For a cell size of 5 km, the maximum round trip delay is around 32 μs or 40 chip periods, and the number of bits required to specify the phase offset between the received signal and the reference clock in unit of

Automatic Threshold Control (ATC)

Like all synchronization systems, a threshold is required to indicate whether synchronization is achieved. If the decision variable at the output of the correlator is greater than the threshold, synchronization is declared. Thus, the probabilities of false alarm and detection is determined by the threshold level. An automatic threshold control is then used to ensure an optimal threshold setting [13]. Many different types of automatic threshold control units are proposed and their performance is also presented in the literature [13], [14]. In this thesis, we assume that the threshold setting is optimal during the analysis of the reverse link synchronization time.

2.3 Analysis of the Reverse Link Synchronization Time

The motivation for quasi-synchronizing the reverse link transmissions is to reduce the multiple access interference and, thus, increase the capacity of a CDMA system. A simple scheme for synchronizing the reverse link transmissions to within 1/2 chip is given in Figure 2.2 and Figure 2.6 of the previous section. The reduction of MAI is realized only when the reverse link synchronization is achieved. So, in this section, we analyze the time required to synchronize the reverse link transmissions.

Two systems are considered in the analysis, namely the non-coherent synchronization system and the coherent synchronization system. The non-coherent synchronization is typically used in the mobile cellular systems where carrier phase of the received signals varies too rapidly to be tracked. Coherent synchronization can be realized in a WLL system for the following reasons: Firstly, PN code acquisition is achieved before the attempt to synchronize the transmissions of subscriber terminals. Therefore, a sequence of training bits can be used to estimate the carrier phase of the received signal. Secondly, because both the base station and the subscriber terminals are stationary and line of sight communication exists in a WLL system, carrier phase of the received signal varies very slowly so that a phase lock loop is able to track

phase estimation [15].

2.3.1 Synchronization Time Analysis

We define the reverse link synchronization time as the time elapsed since the initial PN acquisition is achieved until the received signal is aligned with the reference signal to within 1/2 chip at the base station. Since re-synchronization of the received signal is done 64 chips after the base station sends out the control command, the synchronization time is equal to 64 chip time plus the time taken for re-synchronizing the received signal with the correct adjustment. Synchronization is declared when the correct code phase of the received signal is acquired. On the other hand, if a code phase is erroneously chosen by the synchronization system, a false alarm occurs. Thus, the synchronization time is a random variable and is related closely with the detection and false alarm probabilities. A meaningful characteristic for evaluating the performance of the synchronization system, namely the mean synchronization time, is derived in the below section.

Non-coherent Reverse Link Synchronization

The receiver structure for a non-coherent synchronization system of a DS/BPSK scheme is shown in Figure 2.7.

The received signal is represented by:

$$r(t) = \sqrt{2E_c}c(t + \beta T_c)\cos(wt + \theta) + N(t), \tag{2.2}$$

where β is the received code phase offset, $c(t + \beta T_c) = \sum_n c_n h(t - nT_c + \beta T_c)$ is the spreading code to be acquired, θ is the carrier phase, and E_c is the received chip energy. $h(t)$ is a normalized rectangular chip pulse with period T_c and amplitude $1/\sqrt{T_c}$, and $N(t)$ represents the thermal noise which is a white Gaussian noise process. The components of the signal energy corresponding to the in-phase channel are recovered by correlating $r(t)$ with $\sqrt{2}c(t)\cos wt$, and those of the quadrature channel are similarly recovered by correlating with $\sqrt{2}c(t)\sin wt$. The decision variable R following baseband conversion and integration is then given by

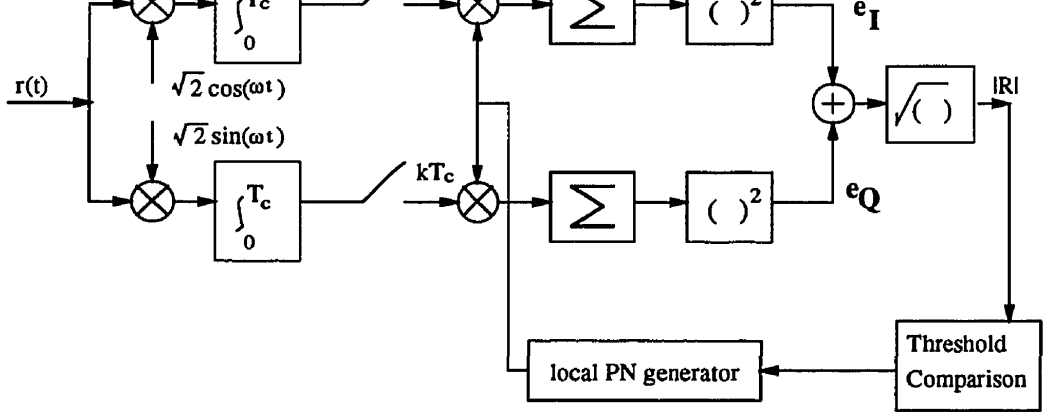

Figure 2.7: I-Q non-coherent synchronizer

$$R_k = \sqrt{e_I^2 + e_Q^2} \tag{2.3}$$

where

$$e_I = Y_k \cos\theta + N'_{I,k}; \quad e_Q = Y_k \sin\theta + N'_{Q,k}, \tag{2.4}$$

and

$$Y_k = \sqrt{E_c} \sum_{n=k-M}^{k} \int_0^{T_c} c(t - nT_c)c(t + \beta T_c - nT_c)dt, \tag{2.5}$$

and

$$\begin{aligned} N'_{I,k} &= \sum_{n=k-M}^{k} \int_0^{T_c} c(t - nT_c)N_I(t - nT_c)dt, \\ N'_{Q,k} &= \sum_{n=k-M}^{k} \int_0^{T_c} c(t - nT_c)N_Q(t - nT_c)dt. \end{aligned} \tag{2.6}$$

$N'_{I,k}$ and $N'_{Q,k}$ are independent, zero-mean Gaussian r.v.'s with variance $\sigma_n^2 = \frac{N_o M}{2}$ and for $M \gg 1$, Y_k is an independent Gaussian distributed sample with mean

$$m = \begin{cases} 0, & \beta > 1 \\ \frac{M\sqrt{E_c}}{4}, & \frac{1}{2} < \beta < 1 \\ \frac{3M\sqrt{E_c}}{4}, & 0 < \beta < \frac{1}{2}. \end{cases} \tag{2.7}$$

tributed uniformly between $\frac{1}{2}$, 1 and 0,$\frac{1}{2}$ respectively.
The variance of Y_k is then given by

$$\sigma_\Delta^2 = \begin{cases} \frac{2E_cM}{3}, & \beta > 1 \\ \frac{7E_cM}{12}, & \frac{1}{2} < \beta < 1 \\ \frac{E_cM}{12}, & 0 < \beta < \frac{1}{2}. \end{cases} \tag{2.8}$$

Now we denote hypothesis H_0 for the code phase offset $\beta > 1$, H_n for $\frac{1}{2} < \beta < 1$, and H_1 for $0 < \beta < \frac{1}{2}$. In hypothesis H_0 and H_n, false alarm occurs if the decision variable, R, exceeds the threshold setting. On the other hand, if the decision variable, R, exceeds the threshold setting in hypothesis H_1, detection is achieved.

Conditioned on Y, the probability density function $f_{H_i}(R|y)$ for the decision variable, R is Rician distributed and is given by [16], [17]

$$f_{H_i}(R|y) = \frac{R}{\sigma_n^2} I_o(\frac{yR}{\sigma_n^2}) \exp\left(-\frac{R^2+y^2}{2\sigma_n^2}\right), \quad R \geq 0 \tag{2.9}$$

where $I_o(x)$ is the modified Bessel function of first kind and zeroth order.
By averaging (2.9) with respect to y, which is a Gaussian r.v., the false alarm probability for $\beta > 1$ becomes

$$P_{fa} = \frac{2\sqrt{1+\rho^2}}{2+\rho^2} \int_{c^*}^{\infty} \exp(-z) I_o\left(\frac{\rho^2}{2+\rho^2} z\right) dz \tag{2.10}$$

where

$$c^* = \frac{V_{Tn}}{4} \frac{2+\rho^2}{1+\rho^2} \tag{2.11}$$

and $\rho = \frac{\sigma_\Delta}{\sigma_n}$ for σ_Δ given in (2.8). V_{Tn} is the normalized threshold equal to $\frac{R_c^2}{\sigma_n^2}$.
The probability of detection is given in [16] as

$$P_d = \int_c^{\infty} \frac{1}{2} I_o(\sqrt{Z}m) \exp\left(-\frac{z+m^2}{2}\right) dz \tag{2.12}$$

where

$$m = \sqrt{\frac{2M\frac{E_c}{N_o}(\frac{3}{4})^2}{1+\frac{E_c}{12N_o}}} \text{ and } c = \frac{V_{Tn}}{1+\frac{E_c}{12N_o}}. \tag{2.13}$$

of detection given in (2.12) with

$$m = \sqrt{\frac{2M\frac{E_c}{N_o}(\frac{1}{4})^2}{1+\frac{7E_c}{12N_o}}} \text{ and } c = \frac{V_{Tn}}{1+\frac{7E_c}{12N_o}}. \tag{2.14}$$

Coherent Reverse Link Synchronization

For the coherent synchronization system shown in Figure 2.6, the in-phase signal energy is recovered by correlating the received signal in (2.2) with $\sqrt{2}c(t)cos(wt+\widehat{\theta})$. $\widehat{\theta}$ is the estimate of the carrier phase, and assuming perfect carrier phase estimation (i.e. $\widehat{\theta}=\theta$), the decision variable at the output of the correlator at time k is then given by

$$Z_k = Y_k + N'_k, \tag{2.15}$$

where

$$Y_k = \sqrt{E_c}\sum_{n=k-M}^{k}\int_0^{T_c} c(t-nT_c)c(t+\beta T_c-nT_c)dt, \tag{2.16}$$

and

$$N'_k = \sum_{n=k-M}^{k}\int_0^{T_c} c(t-nT_c)N(t-nT_c)dt, \tag{2.17}$$

N'_k is a white Gaussian noise sample with variance $\sigma_n^2 = \frac{N_oM}{2}$ and Y_k is an independent Gaussian distributed sample with variance and mean given in (2.7) and (2.8). The decision variable Z_k is also a Gaussian variable with mean m and variance $\sigma_n^2+\sigma_\Delta^2$. The probability of false alarm for $\beta > 1$ is given by

$$P_{fa} = \frac{1}{2}\text{erfc}\left(\frac{V_T}{\sqrt{2(\frac{N_oM}{2}+\frac{2E_cM}{3})}}\right), \tag{2.18}$$

and for $\frac{1}{2} < \beta < 1$

$$P'_{fa} = \frac{1}{2}\text{erfc}\left(\frac{V_T-\frac{M\sqrt{E_c}}{4}}{\sqrt{2(\frac{N_oM}{2}+\frac{7E_cM}{12})}}\right). \tag{2.19}$$

The probability of detection when half chip synchronization is achieved is given below

$$P_d = \frac{1}{2}\text{erfc}\left(\frac{V_T-\frac{3M\sqrt{E_c}}{4}}{\sqrt{2(\frac{N_oM}{2}+\frac{E_cM}{12})}}\right). \tag{2.20}$$

hypothesis H_n at different threshold settings are plotted in Figure 2.8, Figure 2.9, and Figure 2.10 respectively. For hypothesis H_0, the false alarm rate increases with higher SNR as a result of the increase in the variance of the self-noise component σ_Δ^2 in the decision variable. The SNR we are interested in is 5 dB bit energy to noise ratio. With processing gain of 128, we translate the required $\frac{E_b}{N_o}$ to be equal to -16 dB chip energy to noise ratio. At E_c/N_o = -16 dB, we see that the coherent system outperforms the non-coherent scheme. This result is justified because at low SNR, the thermal noise dominates the decision process. For non-coherent detection, the thermal noise components always help to cross the threshold and cause high false alarm rate; whereas, the noise components for coherent detection may reduce the magnitude of the decision variable (i.e. when the noise amplitude is negative). Also at low SNR, the false alarm curves tend to become flat because of the domination of thermal noise floor. For hypothesis H_1, it is intuitive that the detection rate increases with higher SNR since the threshold is crossed with higher probability when the mean of the decision variable increases with high SNR. From Figure 2.8, we see that for hypothesis H_1 the non-coherent scheme performs slightly better than the coherent scheme at low SNR of -16 dB. This again is a result of the higher noise variance for non-coherent detection so that the threshold is crossed with higher probability. The plot of false alarm probability for hypothesis H_n is similar to the plot for detection probability. This is because, for hypothesis H_n, false alarm occurs when the magnitude of the decision variable is higher than the threshold value but the phase offset, β, is between 1/2 and 1. The expression for the false alarm is then given by (2.12) (same expression for probability of detection) with different parameters given in (2.14).

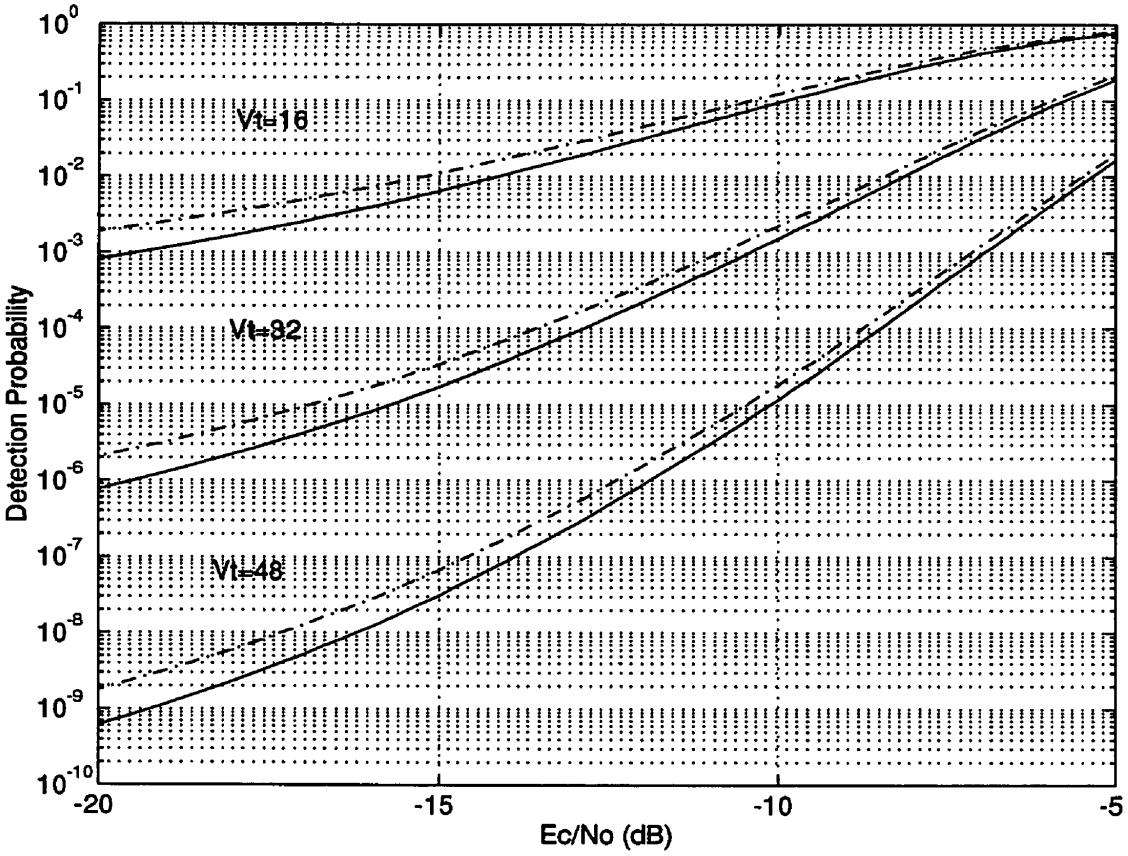

Figure 2.8: Detection probability for coherent(–) and non-coherent(-.) system with different threshold values Vt versus chip SNR. Threshold Vt is normalized to E_c.

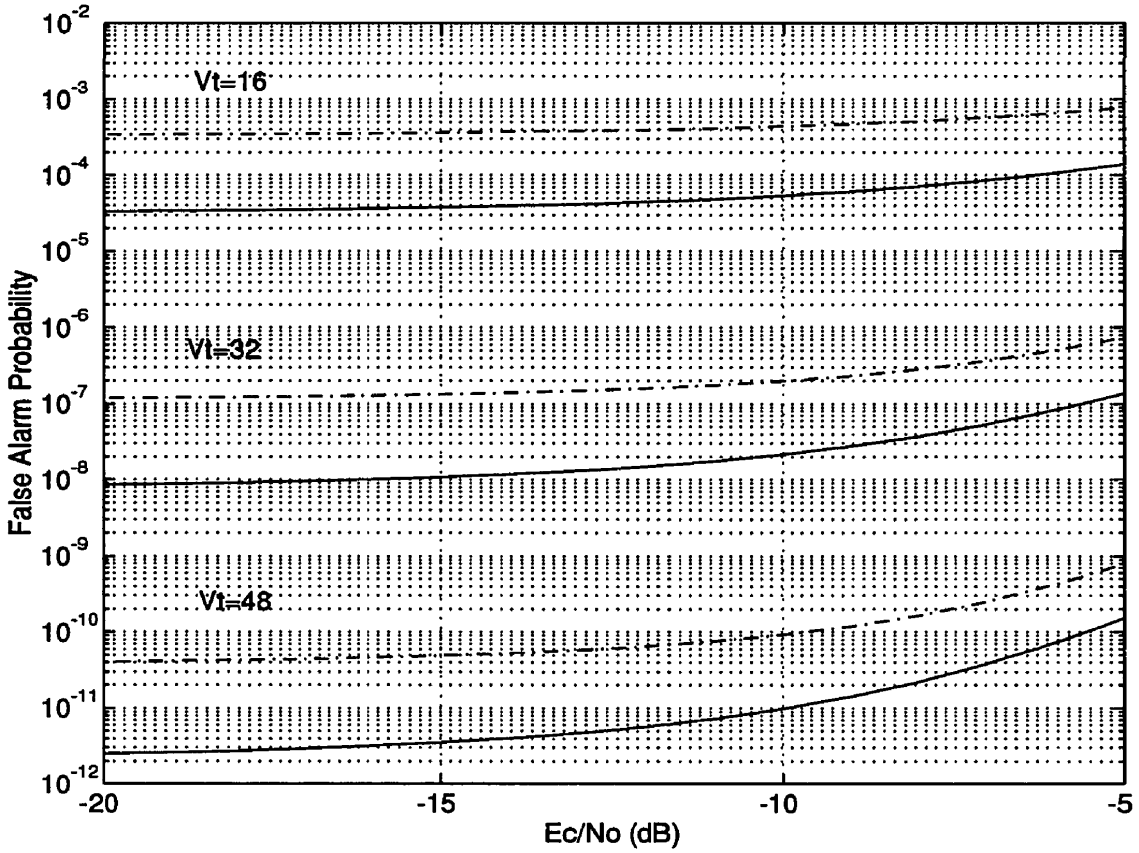

Figure 2.9: False alarm probability for coherent(–) and non-coherent(-.) system and for $\beta > 1$ (hypothesis H_0) with different threshold values Vt versus chip SNR. Threshold Vt is normalized to E_c.

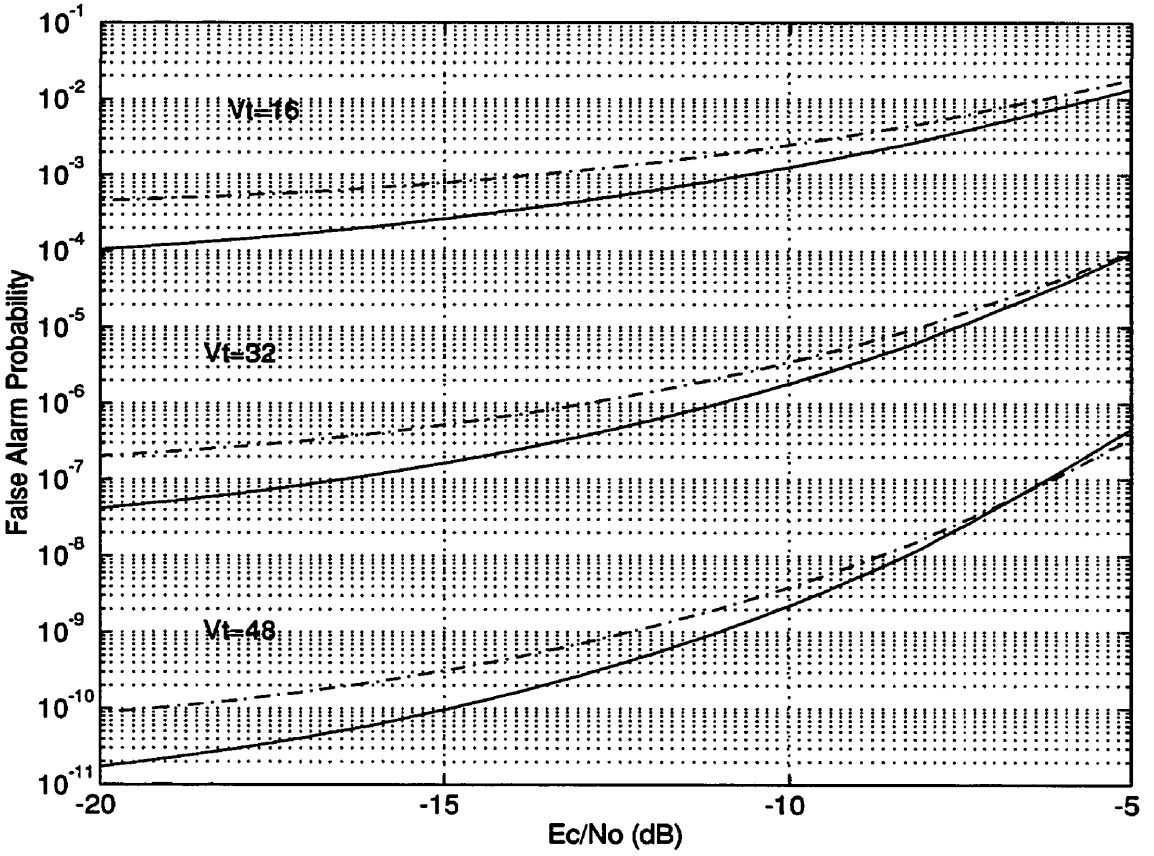

Figure 2.10: False alarm probability for coherent(–) and non-coherent(-.) system and for $1 > \beta > \frac{1}{2}$ (hypothesis H_n) with different threshold values Vt versus chip SNR. Threshold Vt is normalized to E_c.

would be able to find the mean synchronization time. The derivation of mean synchronization time (or acquisition time) was thoroughly studied in [16] and a Markov acquisition model was developed. The mathematical detail is given in Appendix A for reference. Since synchronization is achieved only if the offset β is less than one half of a chip period, an extra gain branch (H_n) is needed to incorporate the false alarm for $1/2 < \beta < 1$. Assuming the use of serial searching scheme, the modified flow graph is given in Figure 2.11. The generator function for the case that the code phase is uniformly distributed in the uncertain region is given by

$$\begin{aligned} P_{ACQ} &= \frac{1}{m}\left(\frac{H_1(z)H_0^{m-2}(z)H_n^2(z)}{1-H_m(z)H_0^{m-3}(z)H_n^2(z)}\right. \\ &\quad + \frac{H_1(z)}{1-H_m(z)H_0^{m-3}(z)H_n^2(z)} \\ &\quad \left. + \frac{H_1(z)H_n(z)}{1-H_m(z)H_0^{m-3}(z)H_n^2(z)} \sum_{i=2}^{m-1} H_0^{m-i-1}(z)\right), \end{aligned} \tag{2.21}$$

where m denotes the number of uncertain cells. The first term of (2.21) is the transfer function associated with the path starting from state $i = 1$ to state ACQ. The second and third terms are then the transfer functions associated with the paths starting from state $i = m$ and any states, $i \neq 1$ and $i \neq m$, to ACQ, respectively.

For a single dwell system, we set

$$H_{nfa}(z) = (1 - P_{fa})z^{\tau d} \tag{2.22}$$

$$H_{fa}(z) = P_{fa}z^{\tau d} \tag{2.23}$$

$$H_p(z) = z^{J\tau d} \tag{2.24}$$

$$H_1(z) = P_d z^{\tau d} \tag{2.25}$$

$$H_M(z) = (1 - P_d)z^{\tau d} \tag{2.26}$$

$$H_0(z) = (1 - P_{fa})z^{\tau d} + P_{fa}z^{(1+J)\tau d} \tag{2.27}$$

$$H_n(z) = (1 - P'_{fa})z^{\tau d} + P'_{fa}z^{(1+J)\tau d} \tag{2.28}$$

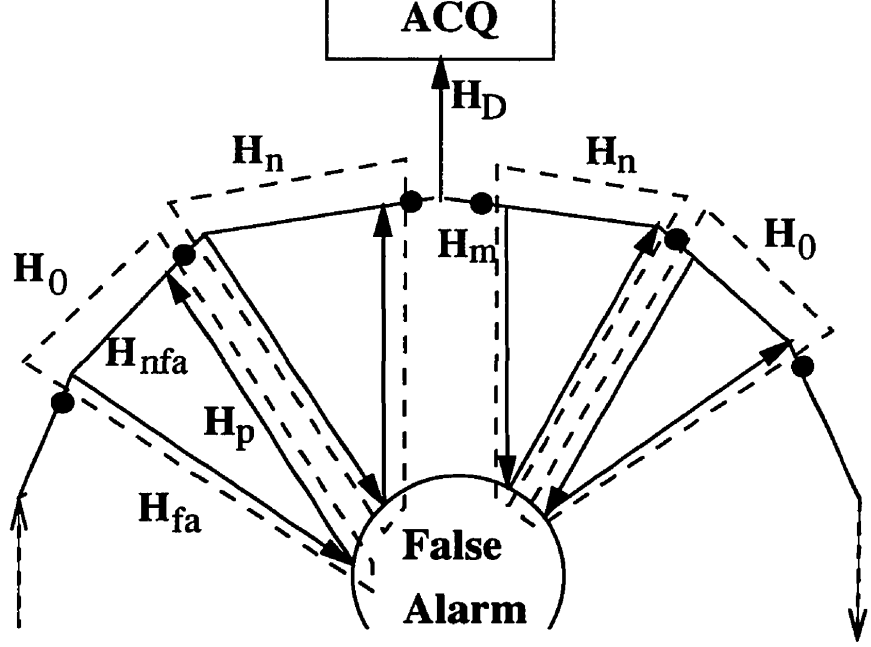

Figure 2.11: Modified flow graph for single dwell serial search acquisition

The mean synchronization time for the system is then given by differentiating equation (2.21) and evaluating it at $z = 1$. The following system parameters are assumed for the analysis of mean synchronization time:

- system bandwidth = 1.25 MHz. Chip rate for the CDMA system is 1.2288 Mcps, which corresponds to chip period of $\approx 0.8\mu$s, and data rate is 9600 bps. This yields a processing gain of $M = 128$.
- maximum cell radius = 5km.
- the number of cells in the uncertainty region $m = 40$ which corresponds to maximum single trip propagation delay of 20 chips or 16μs (delay = 3μs/km).
- observation period $T_u = 64$ chips.
- penalty for false alarm = 100*128 cells which correspond to 100* 64 chip period. When a false alarm occurs, the system is required to redo the initial acquisition before the attempt to synchronize to the transmitter clock again.

late the optimal threshold which yields the minimum mean synchronization time for each SNR value. Normalizing the synchronization time by the observation period T_u, we plot the normalized minimum synchronization time in Figure 2.12. Comparing with the conventional non-coherent scheme, we observe a 3dB improvement for using coherent synchronizer at normalized mean synchronization time of 200. Also at the SNR of interest ($\frac{E_c}{N_o}$ = -16 dB), the mean acquisition time for coherent scheme is half of that required by non-coherent scheme. The advantage of using coherent synchronization system becomes more significant at very low SNR because the false alarm rate for non-coherent system is much higher than that for coherent scheme. Thus, the expensive penalty time required to re-initialize the synchronization procedure accounts for the longer mean synchronization time.

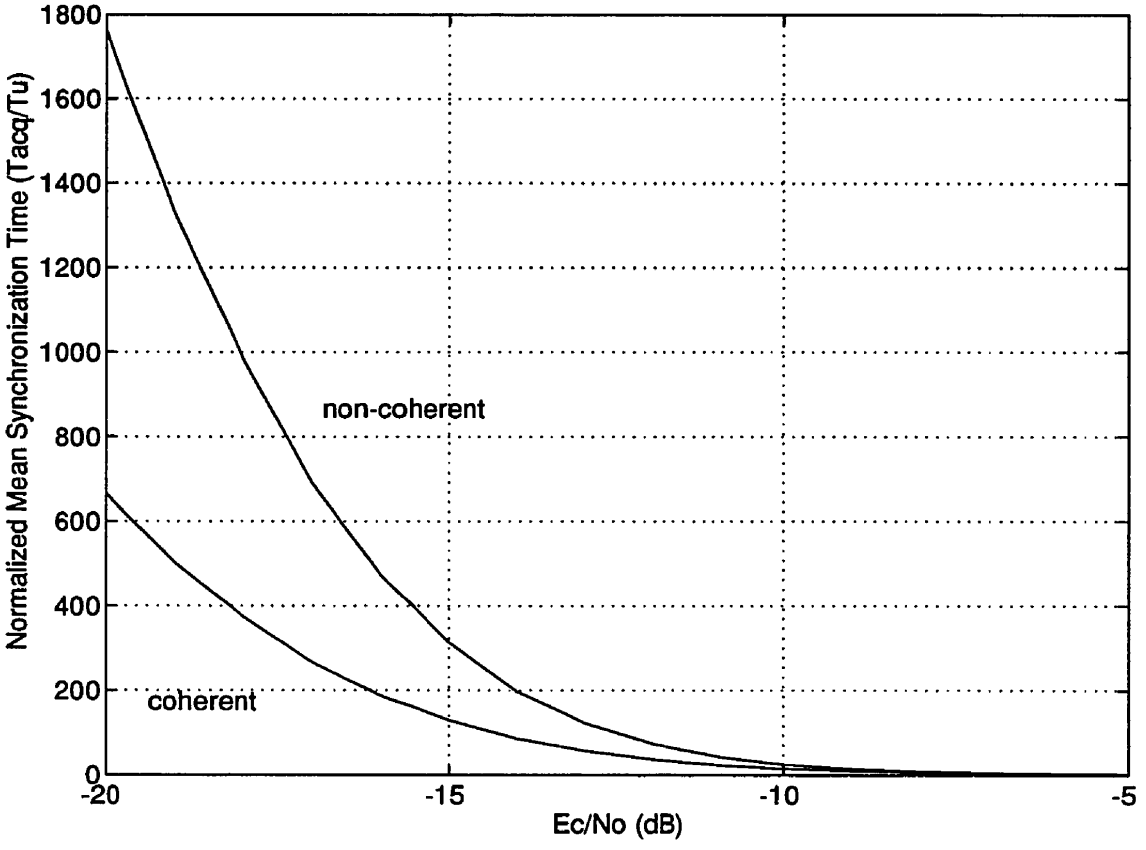

Figure 2.12: Mean synchronization time vs. SNR

Mean synchronization time for a coherent synchronization system is shown in Figure 2.12, and its superior performance over non-coherent scheme is demonstrated. Also, LOS communication is assumed to exist all time during the synchronization process; we assume the use of coherent reverse link synchronization system for the rest of the chapter.

In a CDMA system, the effect of MAI further deteriorates the system performance. In general, it also increases the synchronization time due to the additional interference, which causes more false alarm. As shown in Chapter 1, MAI is modeled as zero-mean Gaussian r.v.'s with variance given by (1.6). Thus, the interference can be treated as another independent Gaussian noise term. The decision variable Z_k in (2.15) is again a Gaussian variable with mean given in (2.8) and variance equal to

$$\sigma^2 = \sigma_n^2 + \sigma_\Delta^2 + \sigma_{MAI}^2 \tag{2.29}$$

where

$$\sigma_{MAI}^2 = \sum_{i=1}^{N_u-1} \frac{E_{c,i}M}{3} \tag{2.30}$$

N_u is the number of users in the same cell. $\sigma_n^2 = \frac{N_oM}{2}$ and σ_Δ^2 is defined in (2.8). Assuming that the cell is in its full capacity; i.e. $N_u = 64$. Also with perfect power control, $E_{c,i} = E_c$ for all $i \in [1, 2, ...N_u]$. Taking MAI into account, equations (2.18)-(2.20) become,
for $\beta > 1$,

$$P_{FA} = \frac{1}{2}\text{erfc}\left(\frac{V_T}{\sqrt{2(\frac{N_oM}{2} + \frac{2E_cM}{3} + \frac{M(N_u-1)E_c}{3})}}\right) \tag{2.31}$$

and for $\frac{1}{2} < \beta < 1$,

$$P_f' = \frac{1}{2}\text{erfc}\left(\frac{V_T - \frac{M\sqrt{E_c}}{4}}{\sqrt{2(\frac{N_oM}{2} + \frac{7E_cM}{12} + \frac{M(N_u-1)E_c}{3})}}\right). \tag{2.32}$$

The probability of detection when half chip synchronization is achieved is given below

$$P_d = \frac{1}{2}\text{erfc}\left(\frac{V_T - \frac{3M\sqrt{E_c}}{4}}{\sqrt{2(\frac{N_oM}{2} + \frac{E_cM}{12} + \frac{M(N_u-1)E_c}{3})}}\right). \tag{2.33}$$

Mean synchronization time for the system with consideration of MAI is plotted in Figure 2.13. As is expected, the system performance is greatly deteriorated in an environment with MAI. The normalized mean synchronization time required for a fully loaded system is 3 times longer than the time required for a single user system at E_c/N_o = -15 dB (120 vs. 360). This is a result of the severe interference caused by other users before the new terminal is able to synchronize its transmission with the others. The performance can be improved by increasing the transmit power during the synchronization process. We find that by increasing the transmit SNR by 3 dB, the minimum mean synchronization time is reduced by 50% and it is reduced by 75% if the transmit SNR is 6 dB higher. The disadvantage of increasing transmit power during synchronization process is minimal as the existing users are quasi-synchronized, and by doubling the SNR for the new users, the net effect on system performance is as if two asynchronous users are using the system. The modified mean synchronization time versus different SNR is plotted in Figure 2.13.

2.4 Performance Analysis of a Quasi-Synchronous Reverse Link in CDMA WLL Systems

In the previous sections, we have proposed a reverse link synchronization system and studied the mean synchronization time for the reverse link. Up until now, we have intuitively assumed the superior performance of the synchronous reverse link system; this section then gives a detailed performance analysis of a quasi-synchronous reverse link system that employs orthogonal spreading code.

For a DS/BPSK system with N_u transmitters, the received signal at the base station receiver is

$$r(t) = \sum_{i=1}^{N_u} \sqrt{2E_i} d_i(t-\tau_i) p_i(t-\tau_i) \cos(w_c t + \theta_i) + n(t) \tag{2.34}$$

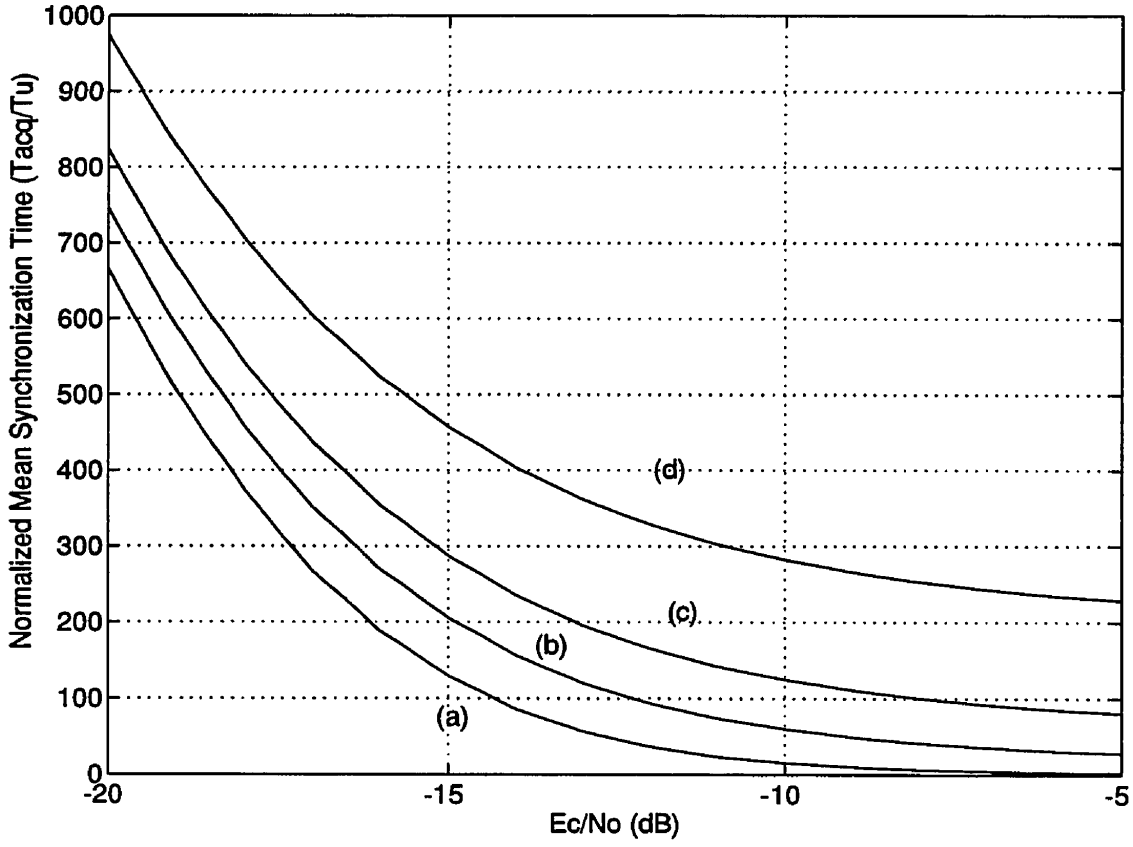

Figure 2.13: mean synchronization time vs. SNR for different situations: (a) no MAI, (b) 6 dB higher in SNR during synchronization process in MAI environment, (c) 3dB higher in SNR during synchronization process in MAI environment, (d) same SNR in MAI environment

where $\sqrt{2E_i}$, $a_i(t-\tau_i)$, $p_i(t-\tau_i) = \sum_n c_{i,n} n(t-nT_c-\tau_i)$, and θ_i are the signal amplitude, time-delayed data signal, time-delayed spreading code sequence, and phase offset of the i th user, respectively, and $n(t)$ is a background thermal noise process with power spectral density $N_o/2$. If we denote T_b be the bit period and T_c be the chip period, then the processing gain is $M = T_b/T_c$. Assuming the use of rectangular chip pulse, the output of the coherent detector is

$$y = \pm M\sqrt{E_i} + \psi + \eta. \tag{2.35}$$

The first term in (2.35) is the desired signal component, ψ is the interference due to the other users, and η is a Gaussian random variable due to thermal noise. Assuming that the delays τ_i are uniformly distributed between $[-\Delta_{max}T_c, \Delta_{max}T_c]$, from Section 1.2.2, the MAI term ψ can be modelled as having zero mean Gaussian distribution when the processing gain $M \gg 1$. The variance is given as

$$\sigma^2 = \frac{1}{2}(1 - \Delta_{max} + \frac{2}{3}\Delta_{max}^2) \sum_{i=1, i\neq k}^{N_u} E_{c,i}. \tag{2.36}$$

The probability of bit error as a function of Δ_{max} is given by

$$P_e = \frac{1}{2}\text{erfc}\left(\sqrt{\frac{E_0}{N_o + \gamma\sum_{i=1}^{K-1} E_i}}\right) \tag{2.37}$$

where

$$\gamma = \begin{cases} \frac{1-\Delta_{max}+\frac{2}{3}\Delta_{max}^2}{M} & \text{for random sequence} \\ \frac{2\Delta_{max}^2}{9M} & \text{Sylvester sequence} \end{cases} \tag{2.38}$$

and E_i is the bit energy for user i; $E_i = ME_{c,i}$. The Sylvester sequences are found to be the best performed spreading codes (i.e. minimum average cross-correlations between different orthogonal codes) in a quasi-synchronous systems [18], and the interference reduction factor, $\gamma = \frac{2\Delta_{max}^2}{9M}$, is also derived by the same author in [12]. Figure 2.14 and 2.15 show the probability of error versus SNR under different environments. It is worth to note that the above performance analysis is done for an uncoded system. Also, we only consider interference created by users in the same cell. A more detail performance analysis is carried out through simulation in Chapter 4. From Figure 2.14, we can see that the system employs synchronous transmissions with

sion by over 10 dB even at BER=10^{-2} [2]. The advantage of synchronous transmission becomes less obvious in a multipath environment (Figure 2.15). This agrees with the comment made in [19]; the reason for the loss in performance is that in a synchronous system, only the first path or the strongest path of all users is synchronized. Thus, other multipaths still interfere with the desired received signal. In this thesis, since we consider WLL systems particularly used in sub-urban area and for the system bandwidth of 1.25 MHz, the channel has only one resolvable path [10].

As we can see in both figures, if all users are synchronized to $\frac{1}{4}$ of a chip period, the performance is virtually as good as a perfectly synchronized system. Also for the probability of error of interest (i.e. $P_e = 10^{-3}$), half chip synchronization is less than 1 dB worse in system performance. Half chip period was chosen as a design parameter over $\frac{1}{4}$ period because, as shown in the Section 1.2.2, $\frac{1}{4}$ period synchronization subscriber system requires a driving clock signal of 4 times the chip frequency. Also, synchronization would have become more difficult if we had set the maximum code phase offset to approach 0.

2.5 Summary

In this chapter, we have studied the advantage of using orthogonal spreading code in the quasi-synchronous reverse link. We find that at $BER = 10^{-2}$, the asynchronous system requires an additional 10 dB in SNR to achieve the same bit error rate. The lower SNR requirement is a result of reduction in multiple access interference by employing orthogonal spreading codes. Although for WLL system with chip rate of 1.2288 Mcps, synchronizing all users to within a small fraction of chip period may be feasible, in order to reduce the complexity of the additional synchronization scheme, 1/2 chip synchronization is chosen. In fact, as shown in Figure 2.14, at the bit error rate of 10^{-3} required to provide acceptable speech quality, the performance of 1/2 chip synchronous system is within 1 dB to the performance of an optimal system.

In section 2.2, we propose a simple way to achieve 1/2 chip synchronization among user transmissions. The additional synchronization time is critically dependent on

[2] we cannot compare performance of the two systems at BER = 10^{-3}.

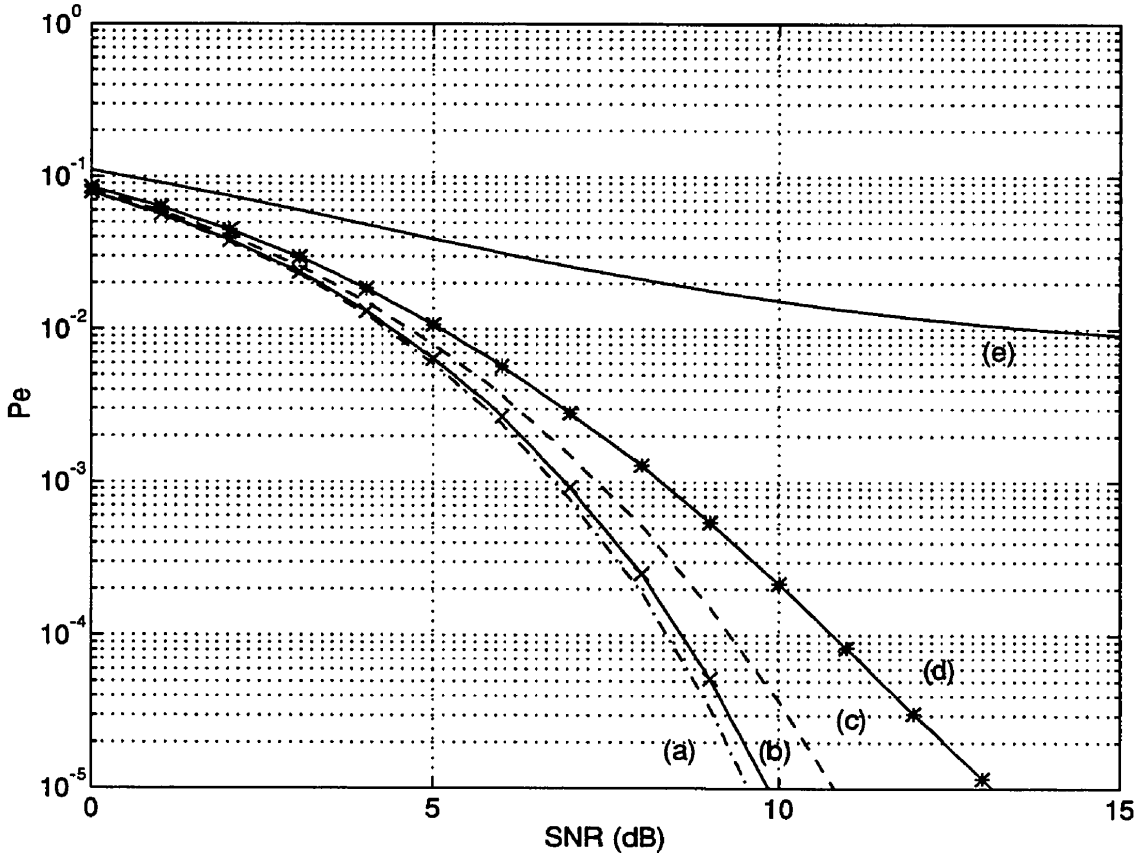

Figure 2.14: P_e versus E_b/N_o for (e) random sequence, (d) quasi-orthogonal with maximum offset equal 3/4, (c) 1/2, (b) 1/4, and (a) orthogonal sequence with N=128, K=64.

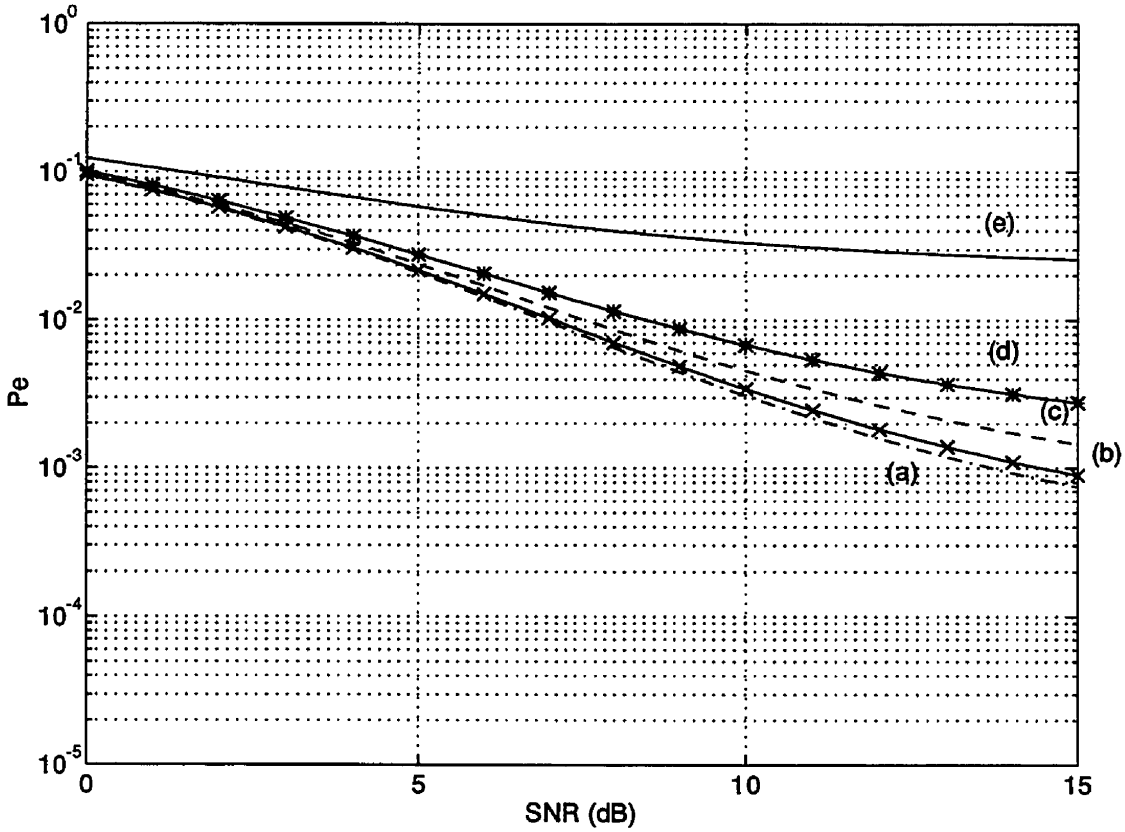

Figure 2.15: P_e versus E_b/N_o for (e) random sequence, quasi-orthogonal with maximum offset equal (d) 3/4, (c) 1/2, (b) 1/4, and (a) orthogonal sequence with same parameters under two-multipaths propagation environment with SNR in the second path 3dB lower than the LOS path.

non-coherent scheme; at E_c/N_o = -16 dB, the mean synchronization time for using coherent system is 200*64 μs, and it is equal to 500*64 μs for using non-coherent system. The effect of MAI on system performance is investigated in Section 2.3.2; compared to a single user system, there is a 3 fold increase in synchronization time for a WLL system with 64 users. The synchronization time in a MAI environment is reduced by one half if we double the transmit power during the synchronization process.

In conclusion, the performance of system in terms of mean synchronization time is analytically derived in the previous sections. The capacity gain demonstrated in section 2.4 outweighs the cost for additional synchronization time. This is because the mean synchronization time of $\approx$ 13 ms (200*64μs) is not significant compared to a typical service time of 3-20 min per call [20]. Also as we find out in section 2.3.2, the effect of MAI on mean synchronization time can be reduced by allowing transmitting higher SNR during the PN synchronization process. With 3dB higher in SNR during synchronization process, the mean synchronization time is 3dB closer to the optimal performance (i.e. case for no MAI). Thus, the net capacity gain is given by the increase in system capacity for using $\frac{1}{2}$ chips quasi-synchronous system (Section 2.4) with 2 asynchronous users.

Chapter 3

Coding and Modulation for Quasi-Synchronous DS-CDMA WLL System

In the previous chapter, we presented the advantage of using orthogonal spreading codes in a quasi-synchronous WLL system to reduce intra-cell interference. The use of orthogonal sequences results in better bit error rate performance as compared to the asynchronous system employing random spreading sequences. However, there are disadvantages of using orthogonal spreading sequences, namely the hard limit on system capacity and the requirement of reusing the set of spreading codes in the other cells. These disadvantages have caused some concern to use non-orthogonal spreading codes in the forward link of the future CDMA systems to facilitate flexible data rate and mobile transparent hand-off [19]. Nevertheless, in a WLL system with no hand-off requirement, we believe that if we can overcome the hard capacity limit, the use of orthogonal spreading sequences is still advantageous for providing the local loop services. Solutions to increase the capacity barrier are proposed in this chapter.

As mentioned in Section 2.1, the communication channels in a DS-CDMA are represented by unique spreading codes. In an orthogonal system, the maximum number of orthogonal spreading sequences is determined by the spreading factor which in turn depends on the chip rate, W, the data rate, R_d, the constellation size in 2

dimensions, n, and the channel coding rate, R_c. The relationship is then given by

$$\text{Max. number of orthogonal sequences} = \text{spreading factor} = \frac{WR_c}{R_d}\log_2 n. \qquad (3.1)$$

As shown in (3.1), in order to guarantee adequate communication channels, the use of low rate channel coding is not suitable in an orthogonal WLL system. As a result, we use only the best rate 1/2 convolutional code in the quasi-synchronous WLL system. In the asynchronous system, the best rate 1/4 convolutional code is used for comparison.

The disadvantage of using orthogonal spreading codes in the forward link of IS-95 has not attracted much attention because the cell capacity for a IS-95 system was proven to be much less than the capacity limit imposed by the orthogonal system. However, as will be shown later, the cell capacity of a WLL system can potentially be greater than this barrier. This motivates our work to study different schemes that increase the hard limit in the orthogonal system, and one way to increase the spreading factor is to use the high spectral efficiency modulation schemes.

This chapter starts with a detail review of the QPSK modulation scheme used in IS-95. A high spectral efficiency QPSK is then introduced, and the advantages and disadvantages of this modulation are presented. A 16 QAM system is used to generalize the trade-off between higher transmit power and higher number of orthogonal users when using high level constellation schemes. A review of Trellis coded modulation, which is known to provide good coding gain for bandwidth-limited systems, is briefly presented. Finally, a link level simulation for systems employing different modulation and coding schemes is carried out at the end of the chapter.

3.1 Analysis of Modulation Schemes

QPSK is a modulation scheme that modulates the data signal to the carriers in two channels, namely the in-phase channel and the quadrature channel. There exist two types of QPSK transmitters: The first kind of QPSK scheme transmits two different information bits in the in-phase and quadrature channels. We will called this scheme a high spectral efficiency QPSK hereafter. The second kind of modulation scheme

quadrature channels, and we will call this the IS-95 QPSK scheme for the rest of this thesis. The advantages and disadvantages of using these two schemes in an orthogonal CDMA system are analyzed in the following sections.

3.1.1 QPSK Modulation in IS-95

The modulation scheme used in IS-95 is called quadrature phase shift keying (QPSK) which transmits the same data bit in both the in-phase and quadrature channels. In an AWGN channel with no MAI, the bit error performance between the QPSK and BPSK modulations scheme is the same. However, in an environment with multiple access interference, the advantages of using the IS-95 QPSK modulation scheme over BPSK are that the inter-chip interference (usually called intersymbol interference [ISI] for nonspread digital demodulation) is reduced by half through the use of independent spreading sequences on the in-phase and quadrature channels; moreover, the variance of interference caused by other users is independent of the relative phase [7] (see also equation (3.8)).

Interchip interference can be eliminated if we employ a chip pulse $h(t)$ such that the match filter output ($g(t) = h(t) * h(t)$ where * is defined as the convolution operator) satisfies the following Nyquist criterion

$$g(nT) = 0 \qquad \text{for integer } n \neq 0, \tag{3.2}$$

where T_c is the chip period. Two examples of pulse shapes that satisfy the above condition are the time limited rectangular pulse and the bandwidth-limited sinc pulse. For a time limited rectangular pulse,

$$h(t) = (1/\sqrt{T_c})[u(t) - u(t - T_c)], \tag{3.3}$$

where $u(.)$ is the unit step function, and a bandlimited sinc pulse is expressed as

$$h(t) = \sqrt{W}\sin(\pi W t)/(\pi W t), \tag{3.4}$$

where $W = 1/T_c$. Since the effect of the interchip interference is, in general, negligible

interference in the following bit error probability analysis.

Bit Error Probability Analysis

The received signal in IS-95 is given as

$$\begin{aligned} r(t) &= \sum_{k=0}^{N_u-1} \sqrt{E_c} x_k(t) p_k^I(t-\tau_k)\cos(\omega_c t+\phi_k) \\ &\quad + x_k(t) p_k^Q(t-\tau_k)\sin(\omega_c t+\phi_k) + n(t). \end{aligned} \tag{3.5}$$

$\sqrt{E_c}$, $x_k(t)$, $p_k^{I,Q}(t-\tau_k) = \sum_n c_n^{I,Q} h(t-nT_c-\tau_k)$, ϕ_k are the signal amplitude, data signal, time-delayed spreading code sequence, and phase offset of the k th user, respectively. $n(t)$ is a background thermal noise process with power spectral density $N_o/2$. $h(t)$ is the chip pulse shape and is normalized such that

$$\int_{-\infty}^{+\infty} h^2(t)dt = 1. \tag{3.6}$$

At time nT_c, the sum of the in-phase and quadrature samples for user 0 after demodulation is equal to

$$\begin{aligned} y_n &= M\sqrt{E_c} \\ &\quad + \frac{\sqrt{E_c}}{2} \sum_{k=1}^{N_u-1} x_{0,n}x_{k,n}\Big(\int_{(n-M)T_c}^{nT_c} p_{0,n}^I(t)p_{k,n}^I(t-\tau_k)\cos\phi_k dt \\ &\qquad + \int_{(n-M)T_c}^{nT_c} p_{0,n}^I(t)p_{k,n}^Q(t-\tau_k)\sin\phi_k dt\Big) \\ &\quad + \frac{\sqrt{E_c}}{2} \sum_{k=1}^{N_u-1} x_{0,n}x_{k,n}\Big(\int_{(n-M)T_c}^{nT_c} p_{0,n}^Q(t)p_{k,n}^Q(t-\tau_k)\cos\phi_k dt \\ &\qquad - \int_{(n-M)T_c}^{T_c} p_{0,n}^Q(t)p_{k,n}^I(t-\tau_k)\sin\phi_k dt\Big) \\ &\quad + N_n. \end{aligned} \tag{3.7}$$

The first term in (3.7) is the desired signal. The second and the third terms are the MAI in the in-phase and quadrature branches, respectively. The thermal noise sample N_n is a zero mean Gaussian r.v. with variance equal to $\mathrm{E}\{(\sum_{n=1}^{M} c_n)^2\}\int_{-\infty}^{+\infty}\frac{N_o}{2}h^2(t)dt =$

are independent ± 1 r.v.'s (i.e. $\mathrm{E}\{x_{0,n}x_{k,n}\} = 0$). The variance for the sum of MAI components equals

$$\begin{aligned}
\mathrm{Var}[I_n] &= \mathrm{Var}[I_n^I] + \mathrm{Var}[I_n^Q] \\
&= \sum_{k=1}^{N_u-1} \frac{E_c}{4} \mathrm{E}\{(\sum_{n=1}^{M} \sum_{m} c_{0,n}^{I,Q} c_{k,m}^{I,Q} \int h(t-nT_c)h(t-mT_c-\tau_k)dt)^2\}[\cos\phi_k + \sin\phi_k]^2, \\
&\quad + \frac{E_c}{4} \mathrm{E}\{(\sum_{n=1}^{M} \sum_{m} c_{0,n}^{I,Q} c_{k,m}^{I,Q} \int h(t-nT_c)h(t-mT_c-\tau_k)dt)^2\}[\cos\phi_k - \sin\phi_k]^2, \\
&= \sum_{k=1}^{N_u-1} \frac{E_c}{2} \sum_{l=n-m} \mathrm{E}\{(\sum_{n=1}^{M} c_{0,n}^{I,Q} c_{k,n+l}^{I,Q})^2\} \mathrm{E}\{g^2(lT_c - \tau_k)\}. \qquad (3.8)
\end{aligned}$$

Without loss of generality, we have assumed that the carrier phase and the delay for user 0 are zero in the above equation. We have also assumed that $\mathrm{E}\{(\sum_{n=1}^{M} c_{0,n}^{I} c_{k,n+l}^{I})^2\} = \mathrm{E}\{(\sum_{n=1}^{M} c_{0,n}^{I} c_{k,n+l}^{Q})^2\} = \mathrm{E}\{(\sum_{n=1}^{M} c_{0,n}^{I,Q} c_{k,n+l}^{I,Q})^2\}$. Also, in the last step of (3.8), $g(t) = h(t) * h(-t)$ where $*$ denotes the convolution operator. Since we have assumed that the received signals are synchronized to within half of a chip time, the residual offsets, τ_k are uniformly distributed between $-1/2T_c$ and $1/2T_c$. In addition, $E\{(\sum_{n}^{M} c_{0,n}^{I,Q} c_{k,n+l}^{I,Q})^2\} = 0$ for $l = 0$ and for $k \neq 0$. If we assume the use of rectangular chip pulse, then $g(t) = 0$ for $|t| \geq T_c$. Also if we assume the use of Sylvester orthogonal spreading code, the expectation of the correlation term in (3.8) is equal to $2M/3$ [18]. In this case the variance of the MAI components is equal to $ME_c/36$. The probability of bit error is then given as

$$P_e = \frac{1}{2}\mathrm{erfc}\sqrt{\frac{E_b}{N_o + \frac{2}{36M}\sum_{k=1}^{N_u-1} E_{b,k}}} \qquad (3.9)$$

The bit error probability shown above is equal to (2.37); i.e. the bit error performance of the IS-95 QPSK system is equal to the performance for a BPSK/DS-CDMA system. The advantage of using QPSK is to avoid the phase dependence of the MAI signal.

[1] $\mathrm{E}\{x\}$ refers to the expectation of x

The main disadvantage of using orthogonal spreading codes in IS-95 is that it limits the maximum number of users to 64 [2]. In a WLL system that uses orthogonal spreading codes and employs directional antennas, the number of users that the system is able to accommodate with acceptable quality may exceed the hard limit imposed. Therefore, in order to gain more capacity and at the same time preserve the orthogonality among users, we want to increase the spreading factor by transmitting more information bits per symbol. For example, in IS-95, one information bit is transmitted per symbol using QPSK. Using 1/2 convolutional coding, the spreading factor given by (3.1) is equal to 64. However, if we choose to transmit different information bits in the in-phase and quadrature branches, we can transmit a maximum of 2 bits/symbol using QPSK. The spreading factor, in this case, is equal to 128 since the symbol period is double, for achieving the same bit rate of 9600 bps specified in IS-95. As a result, we can potentially accommodate 128 users.

Unfortunately, using this higher spectral efficiency QPSK modulation scheme has some disadvantages: Firstly, if we want to double the maximum number of orthogonal users using the high spectral efficiency QPSK scheme, the in-phase and the quadrature branches have to be assigned the same spreading code. Thus, the signal in the quadrature branch becomes another interference source if the phase estimation is not perfect during the coherent demodulation. Secondly, as shown in (3.12), the MAI is dependent on the relative phase between different received signals. In a WLL system, the trade off for these shortages is acceptable because as demonstrated later, the major factor that limits the capacity for a synchronous DS-CDMA WLL system in a sub-urban area is the limitation of the orthogonal channels. In addition, as the population increases, the multiple access interference becomes less dependent on the carrier phases. Finally, the phase tracking can be achieved in the sub-urban environment with strong LOS.

[2]System chip rate is 1.2288 Mcps and date rate is 9600 bps. With the use of 1/2 convolutional code, the spreading factor is equal to 64

The received signal for the high bandwidth efficiency QPSK scheme is similar to (3.5) except that the in-phase and the quadrature channels carry different signals and the in-phase and quadrature channels are assigned the same spreading sequences; i.e., $x^I(t) \neq x^Q(t)$ and $p^I(t) = p^Q(t) = p(t)$.

The output after demodulation of the in-phase signal for user 0 becomes

$$y_n = \frac{M'\sqrt{E_c}}{2} + I_n^I + \frac{N_o M'}{4} \tag{3.10}$$

where the MAI term equals

$$\begin{aligned} I_n^I &= \frac{\sqrt{E_c}}{2} \sum_{k=1}^{N_u-1} x_{0,n}^I x_{k,n}^I \int_{(n-M')T_c}^{nT_c} p_{0,n}(t) p_{k,n}(t-\tau_k) \cos\phi_k dt \\ &\quad + x_{0,n}^I x_{k,n}^Q \int_{(n-M')T_c}^{nT_c} p_{0,n}(t) p_{k,n}(t-\tau_k) \sin\phi_k dt, \end{aligned} \tag{3.11}$$

and $M' = 2M$ as the symbol period is double for this QPSK scheme. MAI for the quadrature components is similar except that the second term of (3.11) is subtracted from the first term.

The variance of the interference in (3.11) is expressed as

$$\begin{aligned} \mathrm{Var}[I_n] &= \sum_{k=1}^{N_u-1} \frac{E_c}{4} \mathrm{E}\{(\sum_{n=1}^{M'} \sum_m c_{0,n} c_{k,m} \int h(t-nT_c) h(t-mT_c-\tau_k) dt)^2\} [\cos\phi_k + \sin\phi_k]^2 \\ &= \sum_{k=1}^{N_u-1} \frac{E_c}{4} \sum_l \mathrm{E}\{(\sum_{n=1}^{M'} c_{0,n} c_{k,n+l})^2\} \mathrm{E}\{g^2(lT_c - \tau_k)\} \mathrm{E}\{(\cos\phi_k + \sin\phi_k)^2\}. \end{aligned} \tag{3.12}$$

The variance is a random variable which is equal to (3.8) in the mean sense. However, the instantaneous variance depends on the relative phase of the received signals. It could be shown that for moderate N_u, $E\{\sum_{k=1}^{N_u} (\cos\phi_k + \sin\phi_k)^2\}$ approaches N_u with high mean to standard deviation ratio. Thus, for a typical WLL system with moderate number of users, the bit error performance for this new QPSK scheme is same as that for the IS-95 QPSK or BPSK schemes.

We now look at the bit error performance for a more practical case; the system uses a bandlimited pulse instead of the rectangular pulse. The chip pulse used in IS-95 closely resembles a square root Nyquist I pulse. Thus, we analyze the bit error

We denote the variance for the correlation of the spreading sequence in (3.12)

$$\mu_l = E\{(\sum_{n=1}^{M'} c_{0,n}c_{k,n+l})^2\} \tag{3.13}$$

and for Sylvester sequences, the values of μ_l for different l are given in [12] as

$$\{\mu_1,\mu_2,\mu_3,\mu_4,\mu_5,\mu_6,\mu_7,\mu_8,\mu_9\} = M'\{2/3,2/3,5/6,2/3,7/8,5/6,7/8,2/3,7/8\}. \tag{3.14}$$

For $l > 9$, $\mu \approx M'$. Since we assume the use of square root Nyquist pulse, $g(t) = h(t) * h(-t) = \text{sinc}(t)$. Assuming that phase offset is uniformly distributed between 0 and Δ_{max}, (3.12) is rewritten as

$$\text{Var}[I_n] = \sum_{k=1}^{N_u-1} \frac{E_c}{4} 2 \sum_l \frac{\mu_l}{\Delta_{max}} \int_{l-\Delta_{max}}^{l} \text{sinc}^2(\tau)d\tau. \tag{3.15}$$

We evaluate the above equation numerically for $\Delta_{max} = 1/2$ and obtain $\text{Var}[I_n] = \sum_{k=1}^{N_u-1} \frac{0.1158E_c}{4}$. Note that we have assumed that for $l > 20$, $\text{Var}[I_n] \approx 0$ as $\text{sinc}^2 t$ decays rapidly to zero for large t.

For a 1/2 chip quasi-synchronous DS-CDMA system employing a sinc chip pulse and QPSK modulation, the probability of error is

$$P_e = \frac{1}{2}\text{erfc}\sqrt{\frac{E_b}{N_o + \frac{0.1148}{M}\sum_{k=1}^{N_u-1} E_{b,k}}} \tag{3.16}$$

3.1.3 High Level Constellation Modulation

It is now obvious that in order to accommodate more users in a WLL system, a high spreading factor is necessary; that is we want a high system bandwidth to symbol rate ratio. This can be achieved by using a modulation scheme with higher dimension constellation. In this section, we examine a system using 16 QAM scheme and 1/2 convolutional code. Figure 3.1 shows a 16 QAM with gray code assignment, which ensures that all adjacent symbols are different only in one bit.

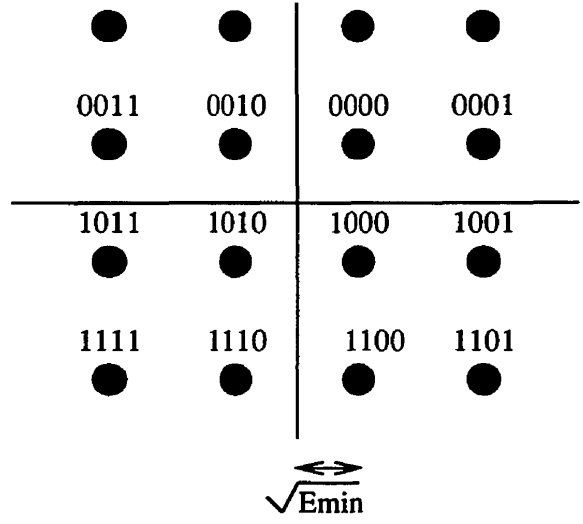

Figure 3.1: 16 QAM with gray code assignment

Bit Error Probability Analysis

The bit error performance of a 16 QAM is determined by the minimum Euclidean distance between symbols in an AWGN channel. Denote the minimum Euclidean distance be $\sqrt{E_{min}}$, the average energy per symbol is equal

$$E_{sym,avg} = \frac{1}{16}\sum_{i=1}^{16} E_{sym,i}. \tag{3.17}$$

Energy per bit is then given by

$$E_{bit,avg} = E_{sym,avg}/4 = \frac{5}{2}E_{min}. \tag{3.18}$$

Equation (3.18) suggests that a 16 QAM scheme requires 5/2 ($\approx$ 3.9 dB) times more energy to achieve the same bit error rate as compared to a QPSK system. The high transmit power for 16 QAM is undesired in a CDMA system since it introduces higher level of both intra-cell and inter-cell interference. The trade-off between the high multiple access interference and the high number of orthogonal spreading codes is determined through simulation carried out in Chapter 4. A link level simulation for the 16 QAM system is carried out in the next section.

As we see from the above discussions, conventional coding schemes, such as the convolutional codes, achieve performance improvement by expanding the bandwidth of the transmitted signal. This has caused a major problem for a system operating in a bandwidth limited channel such as our orthogonal system in which a high spreading factor is necessary to guarantee adequate number of users.

Trellis coded modulation (TCM) has been known to be able to achieve performance gain without expanding the signal bandwidth. It achieves this goal by increasing the number of signal points over the corresponding uncoded system to compensate for the redundancy introduced by the code [21, 22]. The mapping of the coded bits into signal points such that the minimum Euclidean distance is maximized was developed by Ungerboeck based on the principle of mapping by set partitioning [23, 24, 25]. An example of partitioning of 8-PSK channel signals into subsets with increasing minimum subset distances is shown in [25], and the optimum TCM codes for 8-PSK modulation is also given in the articles. In this thesis, we use an 8-PSK TCM encoder with 256 states [3] to compare the coding performance with other coding and modulation schemes. A detail description of the TCM encoder structure and a simulation of the performance in terms of frame error rate are given in the following section.

3.2 Link Level Simulation for Different Modulation and Coding Schemes

3.2.1 System Description

The error control schemes used are the best rate 1/2 convolutional code with constraint length 9 and the best rate 1/4 convolutional code with the same constraint length; the generator polynomials are (561,753) for the 1/2 convolutional code and (463,535,733,745) for the 1/4 convolutional code. The coefficients of the polynomial

[3]The 256 states TCM codes is used so that the complexity of the encoder/decoder is comparable with the 1/2 convolutional code with constraint length 9.

encoder; for example, Figure 3.2 shows the connection of an encoder with polynomial (557).

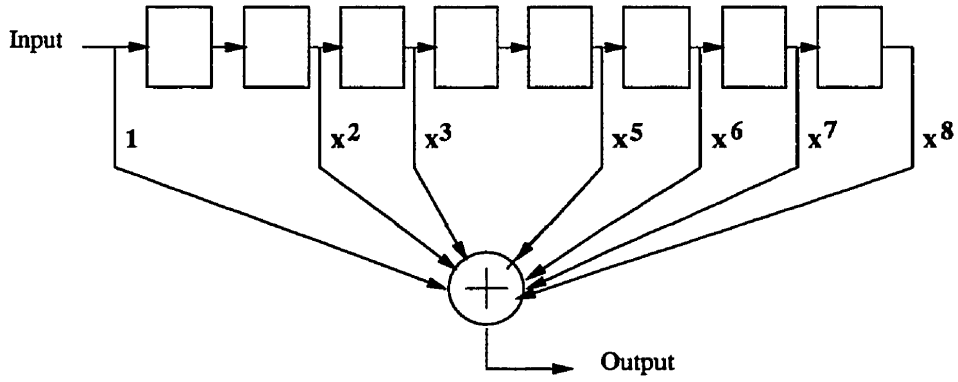

Figure 3.2: Connection for the convolution coder with generator polynomial (557)

The generator polynomial of the rate 2/3 TCM code for 8-PSK modulation is chosen from [25]. The octal representation of the polynomial is (405,250,176) and the encoder structure is shown in Figure 3.3.

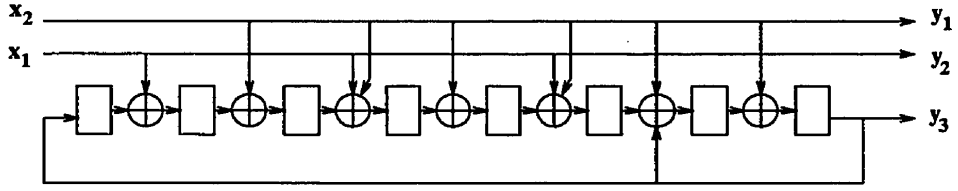

Figure 3.3: Rate 2/3 TCM encoder for 8-PSK modulation

The encoder bits (y_2, y_1, y_0) are then used to choose a signal point shown in Figure 3.4. Again the detail of set partition is given in [25].

Frame error rate is chosen for comparing the performance of different coding and modulation schemes in our simulation; a 20ms frame which consists of 192 bits is considered, and the SINR required to ensure the frame error rate to be less than 0.01 is obtained. Frame error rate is considered a better measure of speech quality than the traditional use of bit error rate since a frame is discarded if errors are found in any bit position [19]. As in IS-95, our speech frame consists of 172 information bits, 12 cyclic redundancy check bits, and 8 convolutional code trailing bits (0 bits).

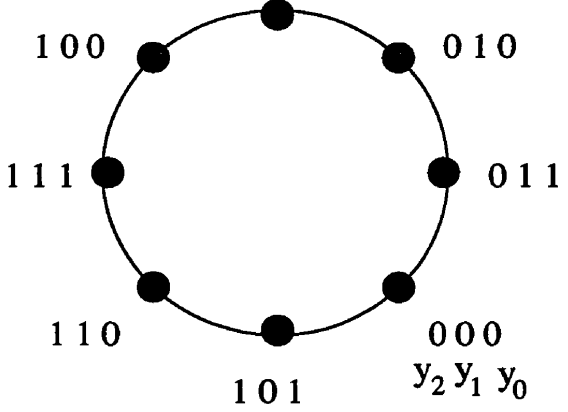

Figure 3.4: Mapping of coded bits to signal points

Channel Error Rate

At the base station, we assume perfect PN code and carrier phase synchronization. The received signals are coherently demodulated and fed to a Viterbi decoder. As given in Section 1.2.2, the interference components at the output of the correlator can be modelled by the Gaussian approximation. The channel error rate for a BPSK or QPSK system is expressed as

$$P_c(\gamma_c) = \frac{1}{2}\text{erfc}(\sqrt{R\gamma_b}), \tag{3.19}$$

where γ_b and R are the source bit energy to noise ratio and the channel coding rate. The channel error rate is then used to find the frame error rate for hard decision decoding in the next section.

3.2.2 Overview of Simulation

Hard Decision Decoding

For every value of γ_b, we find P_c using equation (3.19). Without loss of generality, we generate 300000 all-zero frames and change the encoded bits to "1" with probability P_c. The contaminated bits are then fed to the hard decision Viterbi decoder to obtain the FER. The simulation results for 1/2 convolution and 1/4 convolution coding are shown in Figure 3.5.

To simulate the FER for the system employing soft decision decoding, random Gaussian noise samples are generated with mean

$$m = \sqrt{2\gamma_s R}, \tag{3.20}$$

and variance normalized to 1. γ_s and R are the average symbol energy and coding rate, respectively. For the 16 QAM system, the average bit energy given in (3.18) is used. Metrics in terms of square Euclidean distance are calculated for each trellis path, and the path that gives the smallest metric after shifting in the whole frame (i.e. all 192 bits) is assumed to be the transmitted data sequence. A frame error occurs if any of the 192 bits are non-zero. A plot of the FER versus SINR for the BPSK/QPSK system using 1/2 and 1/4 convolutional code is shown in Figure 3.6. Figure 3.7 shows the FER versus SINR for a 16 QAM system, a QPSK system using 1/2 convolutional code, and a TCM system for 8 PSK modulation. Finally, Table 3.1 and 3.2 summarize the minimum required SINR for achieving $FER < 0.01$ for hard decision and soft decision decoding, respectively.

3.2.3 Discussion of Results

The simulation results are summarized as follows:

- the best rate 1/4 convolutional code has a .5 dB coding gain over the best rate 1/2 convolutional code.
- Soft decision decoding has a 2.5 dB coding improvement over hard decision decoding.
- In Table (3.2), 0.5 dB is added to the minimum required SINR to realize the 8 levels quantization [26].
- For a 16 QAM system, the minimum required SINR to achieve frame error rate of 0.01 is $\approx$ 5.3 dB which is about 3 dB higher than that for the QPSK system. This agree closely with (3.18) which suggests that 16 QAM scheme requires 3.9 dB more energy to achieve the same bit error performance.

1/3 convolutional and orthogonal code	1/2 convolutional code	1/4convolutional code
4.6	4.786	4.286

Table 3.1: Required SINR in dB to achieve $FER < 0.01$ for hard decision decoding

- With trellis coded modulation, the required SINR for achieve $FER < 0.01$ is equal to 3.9 dB.

3.3 Summary

The advantages and disadvantages of different modulation schemes are given as follows:

- The high spectral efficiency QPSK modulation scheme has the same bit error performance as the BPSK or IS-95 QPSK system but it is able to provide twice the number of orthogonal users. The disadvantage of this modulation scheme is that it is sensitive to carrier phase error and the variance of the multiple access interference is dependent on the carrier phases. Fortunately, for a WLL system with moderate users and operated in a LOS environment, these problems are insignificant compared to the advantage of increasing cell capacity.

- The 16 QAM modulation scheme can provide twice the number of orthogonal spreading codes compared to the high spectral efficiency QPSK modulation scheme. However, such scheme requires 3 dB more energy than the QPSK scheme to achieve the same frame error performance. The high transmit power is detrimental in a CDMA system since it incurs high level of intra-cell and inter-cell interference.

- The coded 8-PSK scheme can provide twice the number of orthogonal spreading codes compared to the high spectral efficiency QPSK modulation scheme, and the required SINR to achieve the same frame error performance is only 1.5 dB higher than the QPSK scheme.

Soft decision decoding		
1/2 convolutional code	1/2 convolutional code	1/4 convolutional code
QPSK	16QAM	QPSK
2.935 dB	5.725 dB	2.565 dB

Table 3.2: Required SINR in dB to achieve $FER < 0.01$ for soft decision decoding. † 0.5 dB is added to the minimum required SINR to realize the 8 levels quantization

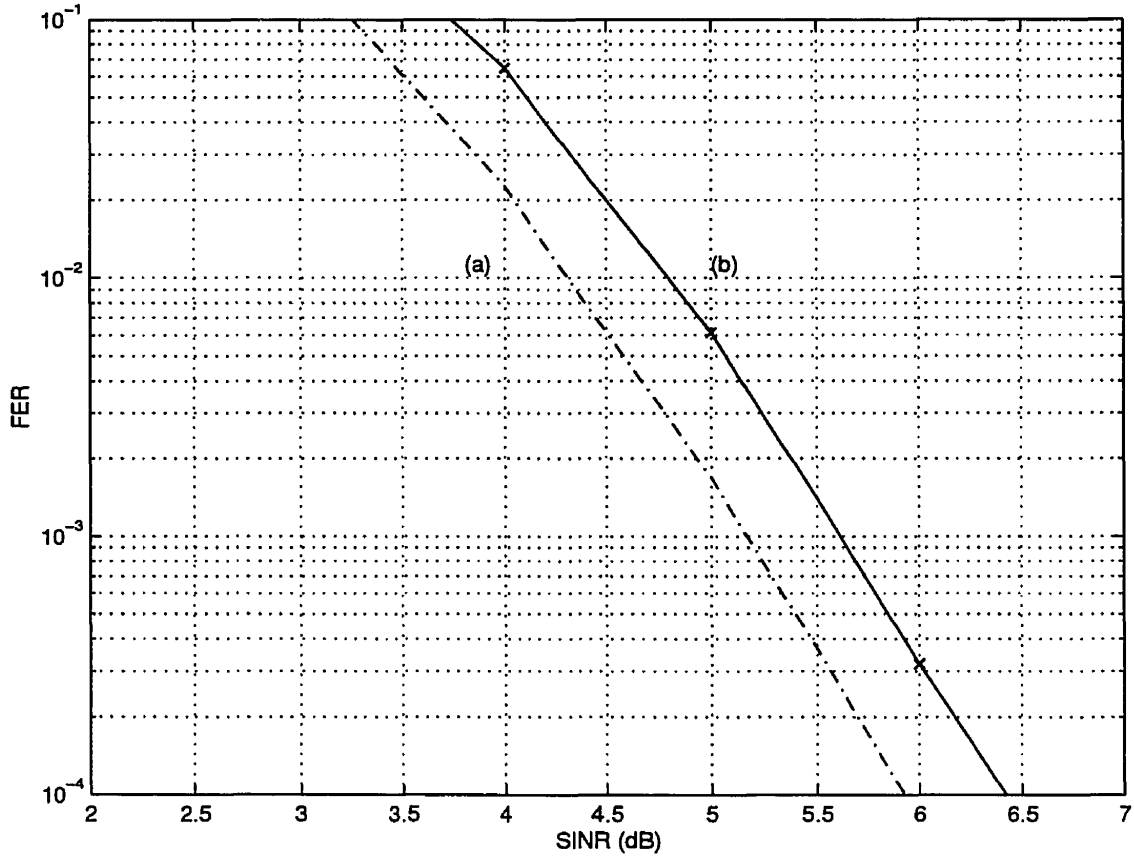

Figure 3.5: SINR vs. FER for different coding schemes with hard decision decoding. (a) (1,4,9) convolutional code, (b) (1,2,9) convolutional code.

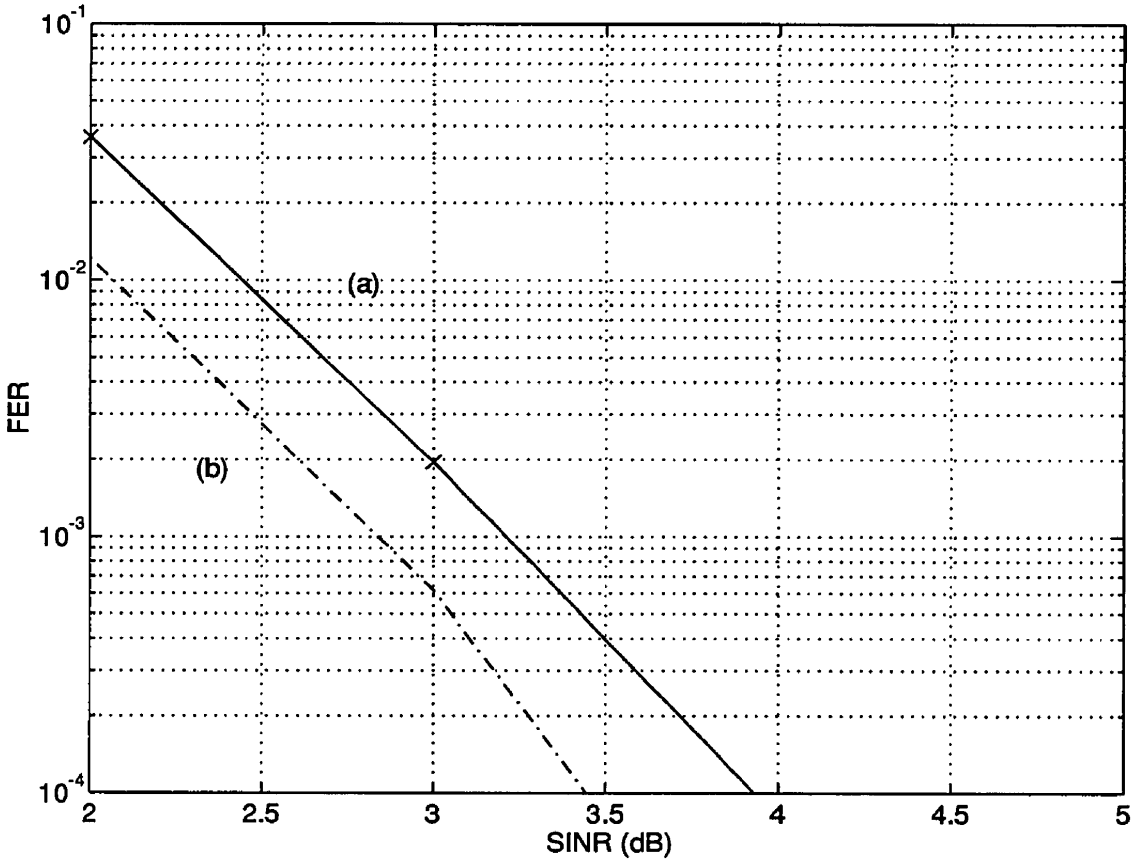

Figure 3.6: SINR vs. FER for different coding schemes with soft decision decoding. (a) (1,2,9) convolutional code. (b) (1,4,9) convolutional code

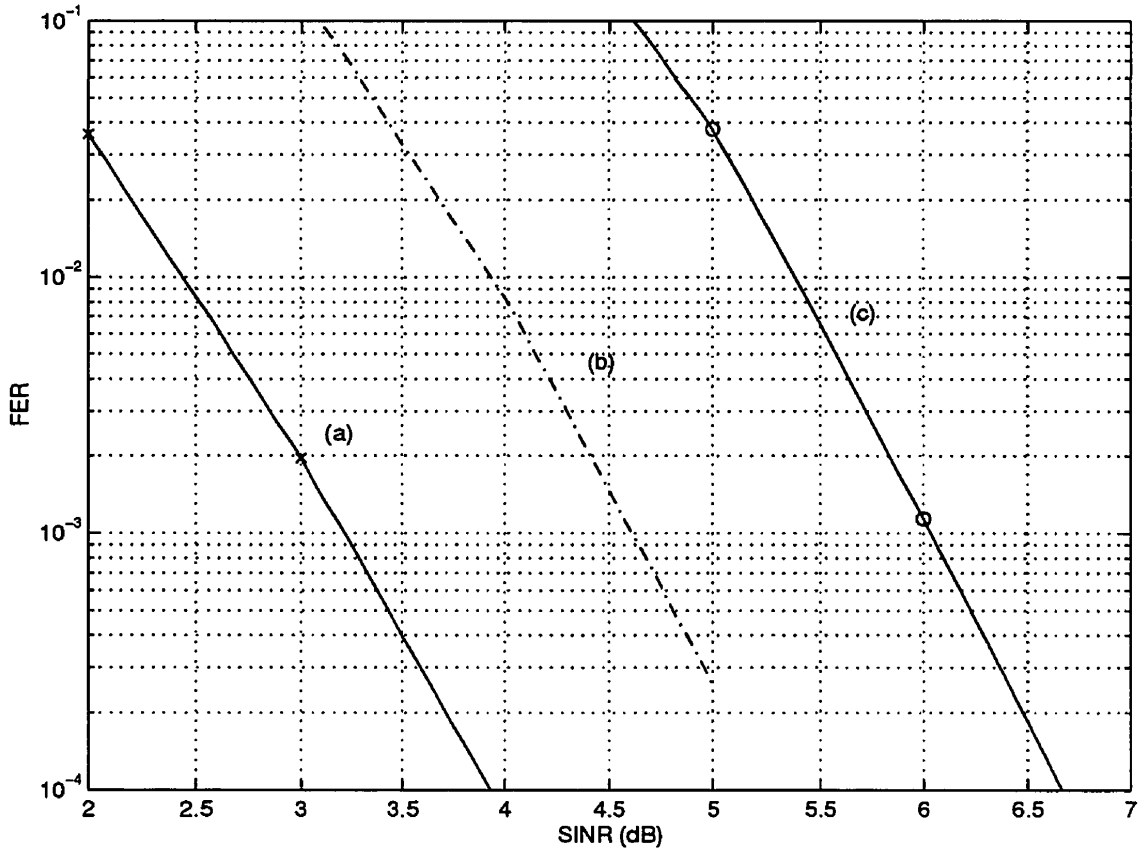

Figure 3.7: FER vs. SINR for different modulation schemes with (1,2,9) convolutional code for the QPSk and the 16 QAM systems. (a) QPSK, (b) rate 2/3 8-PSK trellis coded modulation, (c) 16 QAM

Chapter 4

Overall Capacity of Multiple Cells DS-CDMA WLL Systems

Recall that to obtain high cell capacity for a DS-CDMA WLL system, we want to reduce the MAI. In Chapter 2, we propose to quasi-synchronize the reverse link and assign the users with orthogonal sequences. The use of orthogonal spreading codes has been shown to be very effective in reducing the intra-cell interference and a significant capacity gain is achieved as a result. In a multiple cell WLL system, the inter-cell interference also causes capacity degradation, and this problem, unfortunately, is not alleviated with the use of the orthogonal spreading sequences because of the necessity of reusing the same set of orthogonal sequences in the other cells.

To reduce the inter-cell interference, sectorization is commonly used in many cellular systems. However, as mentioned in Section 1.4, the sector size of a system is limited in order to provide high trunking efficiency. In this chapter, we review another diversity technique, namely the use of directional antennas at the subscriber terminals. This technique is very effective and suitable to reduce inter-cell interference in a WLL system since both the terminals and base are stationary.

In this chapter, we carry out an overall reverse link capacity simulation for a DS/CDMA WLL system. Various channel impairments such as shadowing, multipath propagation, and multiple access interference are considered in the simulation. Simulation results are obtained for various systems (quasi-synchronous and asynchronous systems) employing different modulation and diversity schemes. Finally, a

4.1 Simulation Model

4.1.1 Channel Model and System Description

We now define the channel model that will be used for our simulation in the later sections. The system bandwidth considered is 1.25 MHz; the date rate is 9600 bps and with chip rate equal 1.2288 MHz, the processing gain of the system is 128. The 1.25 MHz system is considered narrow band, and in a suburban area we model the channel by a single resolvable fading path [10]. The path attenuation is modeled as the product of the fourth power of the distance and a log-normal random variable whose standard deviation is 8 dB; i.e. the path loss between subscriber i and the cell site j is proportional to

$$\Lambda_{ij}^2 = \frac{10^{(\xi_{ij}/10)}}{r_{ij}^4}, \tag{4.1}$$

where ξ is a Gaussian random variable with standard derivation $\sigma = 8$ and zero mean, and r_{ij} is the distance between subscriber i and cell site j.

In addition, path attenuation caused by unresolvable multipath propagation is modelled as a Rician random variable, and fading under different environments is simulated by changing the parameter K in the Rician distribution

$$f_{r^2}(u) = (K+1)\exp[-(u(K+1)+K)]I_0(2\sqrt{K(K+1)u}) \tag{4.2}$$

where

$$K = \left(\frac{\mu}{\sigma}\right)^2, \tag{4.3}$$

is the power of the strongest signal to total interference ratio.

A detail description for the reverse link of the proposed system is given below:

- The reverse link transmissions are synchronized to within 1/2 chip period, and the asynchronous reverse link is used for comparison.
- The best rate 1/2 and 1/4 convolution codes described in Section 3.2.3 with soft decision decoding are considered. The required SINR listed in Table 3.2

- The modulation scheme used for the quasi-synchronous system is QPSK described in Section 3.3 which transmits 2 encoded bits per symbol. With the use of rate 1/2 convolution code, the maximum number of orthogonal users in the system becomes 128. For the asynchronous system, the modulation follows IS-95 standard and the rate 1/4 convolution code is used to provide higher coding gain. The 16 QAM modulation scheme and the 8 PSK TCM scheme are also used for comparison.

- Sectorization of 120° is considered. However, to ease the simulation, one sector per cell is assumed for obtaining the capacity defined as the number of users per sector, N_s. The cell capacity for a system with 3 sectors is $3N_s$ users per cell.

- A directional antenna is used at the customer site, and the the energy contained outside the main lobe of the beam is assumed to be negligible. It is intuitive that a very narrow beam directed at the base station (beam angle $\theta \rightarrow 0$) creates the smallest amount of inter-cell interference. However, this is impractical to implement due to the difficulty of aiming exactly in the direction of the base station. Also, as we find out later, the adoption of receiver antenna diversity at the base station is useful to combat the time invariant multipath fading effect. So, a wider beam angle is required to provide independent paths.

4.1.2 Estimation of Reverse Link Capacity

In the past few years, much research has been devoted to finding the reverse link capacity for a DS-CDMA cellular system [27, 28, 29] and the simulation model used in [29] has become a classic to evaluate the system performance. In this chapter, we adopt this model and modify it to incorporate the multipath fading effect and also to realize the use of directional antenna. Our model consists of a grid of $K = 11$ x 11 square cells (Figure 4.1 shows part of the cell layout). We define the capacity as the number of simultaneous users N_s that can be accommodated within a cell, subject to the constraint that the probability of outage is less than 0.01. The outage

of users at any given time is not achieved. Frame error rate (FER) of less than 0.01 is considered acceptable for providing satisfactory speech quality. As in [29], we put N_s users in every cell assuming that they are uniformly distributed over the cell. Then we compute the total interference received at the base station located at the center of the grid labeled as cell 0. The probability $P(FER < 0.01)$ is then computed and we choose the maximum number N_s, subject to the constraint $P(FER < 0.01) < 0.01$.

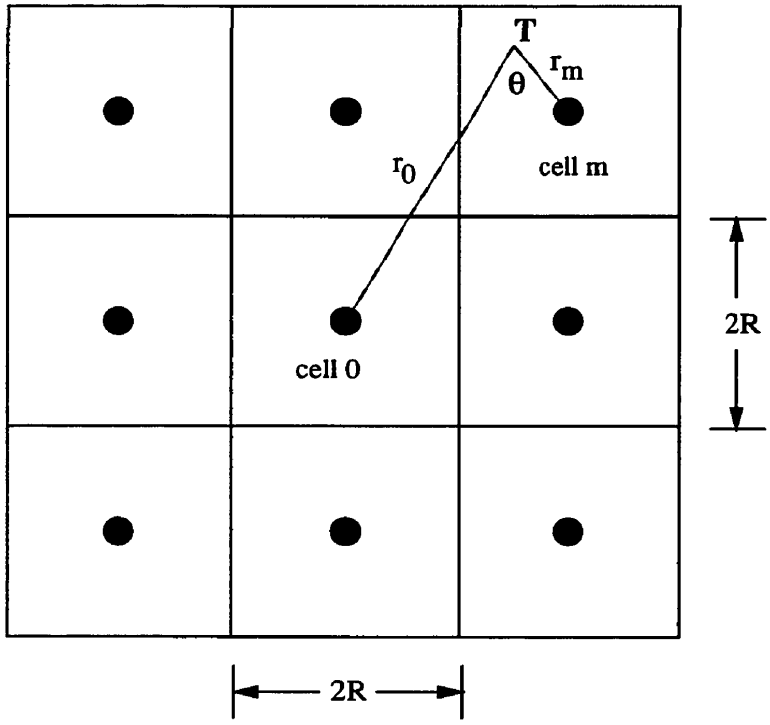

Figure 4.1: Part of cell layout used for simulation (3x3 cells)

Inter-cell Interference Analysis

The inter-cell interference refers to all the unwanted signals transmitted from the terminals of other cells. This interference reduces the signal to interference and noise ratio (SINR) which, in turn, affects the system capacity. In order to find the SINR, we need to know the statistics of this interference. This section presents the derivation of the first and second moment statistics for the inter-cell interference.

Assuming that the received signals in every cell site are perfectly power controlled

ference caused by the i^{th} terminal at cell j is equal to

$$S_{ij} = \frac{x_i^2 \Lambda_{i0}^2}{\Lambda_{ij}^2}, \tag{4.4}$$

where index 0 denotes the cell in the center of the grid where we compute the interference, x_i^2 is the inverse of multipath fading, and Λ_{ij} is defined in (4.1).

The total inter-cell interference is then given by integrating over the two dimensional area covering all the cells except the center cell, *cell* 0 (see Figure 4.1). The interference-to-signal ratio is expressed as [29]

$$I/S = \int\int \psi \left(\frac{r_m}{r_0}\right)^4 10^{(\xi_0 - \xi_m)/10} \Phi(\theta, \xi_o - \xi_m, r_0/r_m) \rho dA \tag{4.5}$$

where ψ is the voice activity variable

$$\psi = \begin{cases} 1, & \text{with probability } \alpha \\ 0, & \text{with probability } 1-\alpha, \end{cases} \tag{4.6}$$

$\rho = N_s/4$ is the density defined as the number of users per unit area, and m is the cell-site index. To simplify the calculation of (4.5), m is chosen to be the smallest distance rather than the smallest attenuation; i.e. we assume that the terminals transmit to the closest base station. The distance between a terminal and base station m, is expressed as

$$r_m = \min_{k \neq 0} r_k. \tag{4.7}$$

The function $\Phi(\theta, \xi_o - \xi_m, r_0/r_m)$ is defined as

$$\Phi(\theta, \xi_0 - \xi_m, r_0/r_m) = \begin{cases} 1, & \text{if } (r_m/r_0)^4 10^{(\xi_0 - \xi_m)/10} < 1 \\ & \text{and } \theta < \phi/2 \\ 0, & \text{otherwise} \end{cases} \tag{4.8}$$

where ϕ is the beam width of the directional antenna and θ is the angle shown in

$$\theta = \cos^{-1}\left(\frac{r_m^2 + r_0^2 - d_{0m}^2}{2r_m r_0}\right) \tag{4.9}$$

d_{0m} is the distance between the base stations at cell 0 and cell m. r_m and r_0 are the distances shown in Figure 4.1.

Since the total inter-cell interference is a sum over large population of i.i.d random variables, by Central Limit Theorem it can be approximated by a Gaussian r.v. with mean and variance given in [29] (anyone interested in the derivation of (4.10-4.13) is referred to [29]). The mean and variance are summarized as follows:

$$\text{mean} = m = \mathrm{E}(I/S) = \alpha \int\int \left(\frac{r_m}{r_0}\right)^4 \mathrm{E}\{x^2\} f\left(\frac{r_m}{r_0}\right) \rho dA, \tag{4.10}$$

where

$$f\left(\frac{r_m}{r_0}\right) = \exp[(\frac{\sigma \ln 10}{10})^2]\left\{1 - Q\left[\frac{40}{\sqrt{2\sigma^2}}\log_{10}\left(\frac{r_0}{r_m}\right) - \sqrt{2\sigma^2}\frac{\ln 10}{10}\right]\right\}, \tag{4.11}$$

and the variance is

$$v = \mathrm{var}(I/S) \leq \int\int \left(\frac{r_m}{r_0}\right)^8 \left[\alpha \mathrm{E}\{x^4\} g\left(\frac{r_m}{r_0}\right) - \alpha^2 \mathrm{E}^2\{x^2\} f^2\left(\frac{r_m}{r_0}\right)\right] \rho dA, \tag{4.12}$$

where

$$g\left(\frac{r_m}{r_0}\right) = \exp[(\frac{\sigma \ln 10}{5})^2]\left\{1 - Q\left[\frac{40}{\sqrt{2\sigma^2}}\log_{10}\left(\frac{r_0}{r_m}\right) - \sqrt{2\sigma^2}\frac{\ln 10}{5}\right]\right\}. \tag{4.13}$$

Note that $Q(x)$ is defined as

$$Q(x) = \frac{1}{\sqrt{2\pi}} \int_x^\infty e^{-t^2/2} dt. \tag{4.14}$$

In a 1/2 chip quasi-synchronous DS/CDMA system employing sinc chip pulse, the interference reduction factor γ, is given as

$$\gamma = \begin{cases} 1, & \text{for asynchronous system} \\ 0.1158, & \text{for 1/2 chip quasi-synchronous system.} \end{cases} \tag{4.15}$$

The reduction factor for 1/2 chip quasi-synchronous system is obtained by evaluating (3.15) numerically.

With also considering the voice activity factor ψ, the total intra-cell interference to signal ratio for a system with N_s users is equal to

$$(I/S)_{intra} = \gamma \sum_{i=1}^{N_s-1} \psi_i. \tag{4.16}$$

Outage Probability

At the base station, the signal to total interference and noise ratio (SINR) is a random variable

$$SINR = \frac{W/R}{\gamma \sum_{i=1}^{N_s-1} \psi_i + (I/S) + (\eta/S)} \tag{4.17}$$

where the mean and variance of I/S are derived in the previous section and have justified taking it to be a Gaussian random variable. The remaining terms W/R is the processing gain, and η/S is the thermal noise to signal ratio.
The outage probability is then obtained as

$$P_{outage} = Pr(FER > 10^{-2}) = Pr\left(\gamma \sum_{i=1}^{N_s-1} \psi_i + I/S > \delta\right) \tag{4.18}$$

where

$$\delta = \frac{W/R}{SINR} - \frac{\eta}{S}. \tag{4.19}$$

Because ψ is binomial distributed and I/β is a Gaussian variable, and all variables are mutually independent. Equation (4.18) can be expressed in close form

$$P_{outage} = \sum_{k=0}^{N_s-1} \begin{pmatrix} N_s - 1 \\ k \end{pmatrix} \alpha^k (1-\alpha)^{N_s-1-k} \mathrm{Q}\left(\frac{\delta - \gamma k - mN_s}{\sqrt{vN_s}}\right) \tag{4.20}$$

where N_s is the number of users per sector, m and v are values defined in (4.10) and (4.12) respectively. γ is then the interference reduction factor for the quasi-synchronous system given in (4.15).

4.1.3 Overview of Simulation

For calculating the mean and variance of the inter-cell interference, the integrations in (4.10) and (4.12) are carried out through Monte Carlo Simulation. 1,000,000 uniformly distributed points are generated in one quarter of the cell layout given in Figure 4.1. Due to the symmetry of the cell layout, the first and second moment statistics of the total inter-cell interference are then equal to 4 times those obtained by the simulation.

To evaluate (4.10) and (4.12), we need to find $E\{x^2\}$ and $E\{x^4\}$. As mentioned in Section 4.1.2, the power gain x^2 is the inverse of the Rician distributed multipath interference. The Rician r.v. is generated as follows:
we first generate the Rician r.v.

$$r = \sqrt{g_1^2 + g_2^2} \tag{4.21}$$

where g_1 is a Gaussian r.v. with mean α and variance σ^2 and g_2 is a Gaussian r.v. with zero mean and variance σ^2. By normalize $E[r^2]$ to 1, that is the average signal power attenuation is only caused by path loss and shadow fading, we have

$$\begin{aligned} E(r^2) &= E(g_1^2 + g_2^2) \\ &= \alpha^2 + \sigma^2 + \sigma^2 \\ &= \sigma^2(\frac{\alpha^2}{\sigma^2} + 2) \\ &= 1. \end{aligned} \tag{4.22}$$

1/2 convolution code	1/2 convolution code	1/4 convolution code	TCM
QPSK	16QAM	QPSK	8 PSK
3.935 dB	6.725 dB	3.565 dB	5.4 dB

Table 4.1: Modified required SINR in dB to achieve $FER < 0.01$ for soft decision decoding with 1 dB implementation margin.

For $K = \frac{\alpha^2}{\sigma^2}$, the variance and mean of the Gaussian r.v.'s in terms of K are given as

$$\alpha = \sqrt{\frac{K}{K+2}} \tag{4.23}$$

and

$$\sigma = \sqrt{\frac{1}{K+2}}. \tag{4.24}$$

Since the transmit power is limited in the subscriber terminal and in order to avoid severe interference induced by users in deep fade, we set the maximum power gain to 10. The power gain x^2 is given by

$$x^2 = \begin{cases} \frac{1}{r^2}, & \text{for } r^2 < 1/10 \\ 10, & \text{otherwise.} \end{cases} \tag{4.25}$$

Finally, the required SINR for evaluating (4.19) is based on the results listed in Table 3.2[1]. A 1 dB implementation margin is added to account for the imperfection of power control, phase estimation error, and the extra interference caused by users not yet synchronized as mentioned in Section 2.5. The SINR used for the simulation is summarized in Table 4.1. The η/S is set to 1 dB which reflects a reasonable subscriber transmitter power level [29]. Finally, the voice activity factor α is set to 0.4.

4.2 Numerical Results and Discussion

The simulation of the reverse link capacity for a CDMA WLL system involves a few parameters; these are parameters such as K which specifies the multipath fading environment, and ϕ which is the beam width of the directional transmitter antenna. A

[1] we only consider soft decision decoding in our capacity simulation

for the WLL system using synchronous and asynchronous transmissions with different modulation and diversity schemes is given at the end.

4.2.1 Receiver Antenna Diversity in Severe Multipath Environment

The parameter K is defined in (4.3) as the strongest signal to total interference ratio for the Rician distribution. The physical meaning of K describes the severeness of the multipath fading environment. For example, when $K \to \infty$, α in (4.23) approaches 1 and σ in (4.24) approaches 0. This corresponds to a no fading environment where only a direct path and a ground reflected path exist between the base station and the subscriber terminal. This kind of environment may exist in the rural area where there is no obstacle around the users. The other extreme case is when $K \to 0$. This corresponds to the case where there is no strong communication path in the reverse link. The fading amplitude then becomes a Rayleigh random variable. This is a typical environment in the urban area where high buildings exist around the customer terminals. Figure 4.2 shows the cumulative distribution function of the power gain variable x^2 for the Rayleigh fading and no fading environment. For the Rayleigh fading environment, over 35% of the population requires power gain larger than 10. The coverage [2]increases to 93% if two receiver antennas are used at the base station, and we select the antenna with higher signal power; i.e. the use of selective antenna diversity improves the coverage by 28%. For environment with no multipath (i.e. $K = \infty$), the power gain is always equal to 1.

Currently the main application of the WLL system is to provide telephone services in the suburban area, and a strong line of sight path between the transmitter and base station usually exists. However, due to the liberalization of the telecommunications services, WLL is also considered by many operators to provide competitive telephone service in the urban area. Thus, performance of the system under both environments is given in the later section.

[2]Coverage is defined as the percentage of population that requires power gain < 10.

Capacity	97	98	99	100	101	102	104	105	107	108

Table 4.2: Maximum number of users per sector for different beam width values

4.2.2 The Use of Directional Transmitter Antenna

The use of directional antenna is an effective way to reduce inter-cell interference. In a CDMA system, most inter-cell interference is caused by transmitters located close to the cell boundary. One way to solve the problem is to lower the transmit power for users at the boundary; however, this is not possible for a CDMA system due to the near-far effect (i.e. signal transmitted at distant location is overwhelmed by signals coming from near the base station). The use of directional transmitter antenna is most suitable for the WLL system since the transmitter knows the direction of the base station. By pointing the beam to its own base station, the transmitter does not create interference to the neighbouring cells. In practice, due to the complexity of antenna structure and the radiation of signal power at radio frequency, the beam width of around 60° is considered reasonable. In addition, the use of antenna diversity in the base station also prevents the use of very narrow beam transmitter antenna. Table 4.2 shows the system capacity versus beam width for an asynchronous system operating in a no fading environment. We find that the maximum number of simultaneous users is decreased by 1 for every 10 degree increase in the antenna beam width.

4.2.3 Overall Reverse Link Capacity for a Quasi-Synchronous CDMA WLL System

The capacity for the asynchronous and synchronous system using omni-directional transmitter antenna are plot in Figure 4.3 and Figure 4.4, respectively. A detail summary of the simulation results for the system capacity is tabulated in Table 4.3 and Table 4.4.

As we can see from both Figure 4.3 and Figure 4.4, the capacity of the local loop system greatly depends on the availability of LOS transmission. For system using non-orthogonal spreading code, the maximum number of simultaneous users per sector is 43 in a no LOS environment and 67 for a LOS environment. Thus,

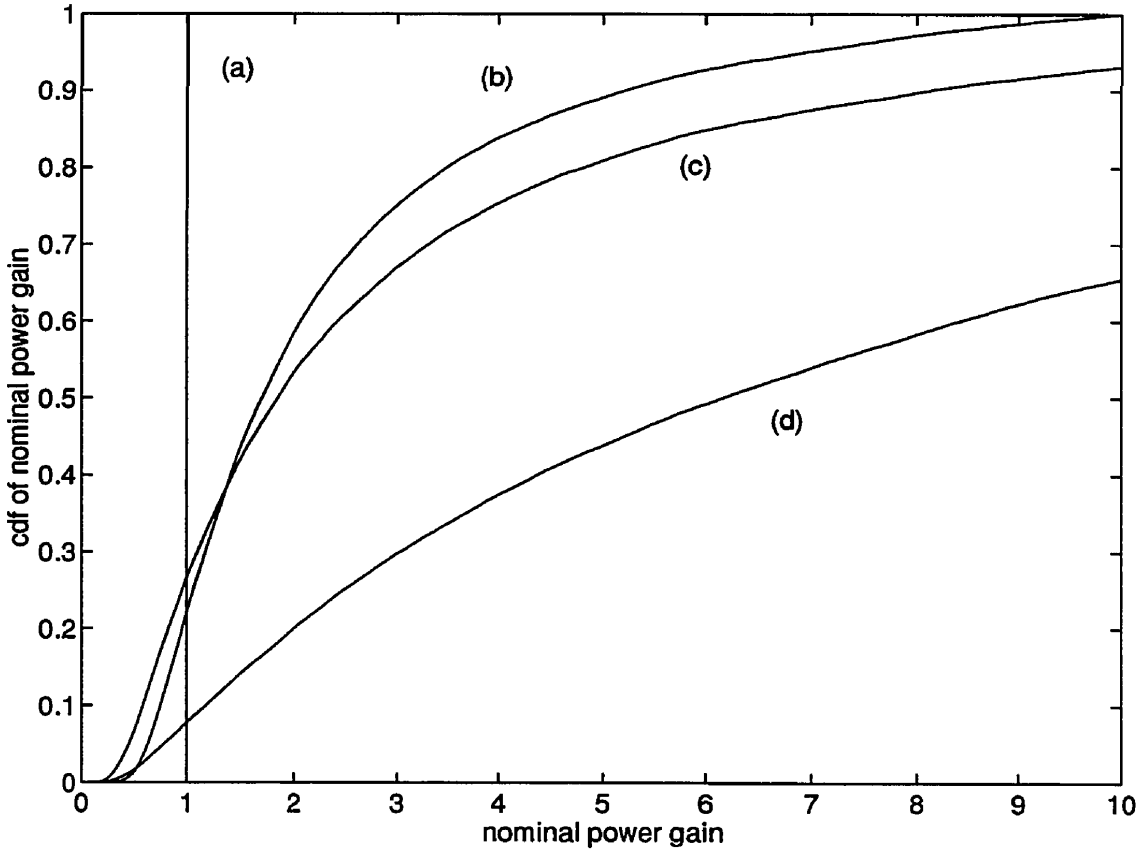

Figure 4.2: CDF of nominal power gain for different fading environments: (a) no fading, (b) Rician fading with K =10, (c) Rayleigh fading with selective antenna diversity (2 antennas), (d) Rayleigh fading with one antenna.

also required to support a high capacity WLL system. The deterioration of system capacity in a non-LOS environment is greatly due to our assumption of perfect power control. The transmit power is controlled to ensure that the power level received at the base station is constant and equal to other received powers from users in the same cell. When the terminal is located in a multipath faded environment, it is requested to transmit at a higher power not exceeding the power limit. As a result, the terminal causes more interference to its neighbouring cells. In addition, the higher variation of power gain in the non-LOS environment also increases the total inter-cell interference expressed in (4.12).

The advantage of using receive antenna diversity at the base station is also illustrated in both plots. For the asynchronous system, the capacity increases by 1.5 dB (from 43 users to 61 users), and for the synchronous system, the capacity increases by 1.7 dB (from 59 to 87 users) in the non-LOS environment. The use of selective antenna diversity greatly reduces the variation of the power gain variable x^2 which not only increases the coverage for the local loop system, but also reduces the effect of large power variation mentioned in the previous paragraph.

In Table 4.3, we discover that the increase in capacity using directional antenna depends on both the beam width and also the operating environment. As shown in Table 4.2, in the strong LOS environment ($k = \infty$), the increase in system capacity is inversely proportional to the the beam width (average of +1.25 users per -10 degree of beam width). However, the relation between beam width and capacity is no longer linear when $K = 0$ (Rayleigh multipath fading environment). The result is +1.66, +2, +3 users per -10 degree beam width at ranges $360^o - 120^o$, $120^o - 60^o$, $60^o - 30^o$, respectively. The inter-cell interference received at cell 0 is reduced proportionally by using narrower beam width transmitter antenna. However, there are also other interference components such as the thermal noise and intra-cell interference which eventually dominate when the inter-cell component is reduced by using directional antenna. This explains why the use of narrower beam width antenna is more effective in a severe fading environment; the total inter-cell interference in this environment is generally larger due to the large power gain variation.

As mentioned in Section 2.1, the use of synchronous reverse link transmission is

able to improve the system performance. The simulation result seems to agree with the statement. First we should note that according to the simulation result, the WLL system has a higher capacity as compared to the IS-95 system; for the asynchronous reverse link transmission in a Rayleigh faded environment, the capacity for the WLL system is 61 users/sector, and for the perfectly power controlled IS-95 system it is 35 users/sector [29]. This is mainly due to the better coding performance in the static channel, which has translated to the increase of system capacity. In a LOS environment (Table 4.3), we can see an almost double in capacity for system employing synchronized reverse link transmission. The performance gain reduces to 37% in a severe multipath environment. Since the advantage of employing the orthogonal spreading sequences is to reduce the intra-cell interference, the performance of a synchronous system is less superior when the dominated noise components are the inter-cell interference. Finally, we observe that by employing narrower beam width transmitter antenna, the performance between the synchronous and asynchronous system becomes comparable. This is due to the hard limited number of orthogonal users in the synchronous system (128 for our case). Should there be no hard limited in the synchronous system, the cell capacity for the system could be a lot higher; for example without the hard limit, the local loop system with QPSK modulation, employing one antenna and a 120° beam width transmitter, can support up to 216 users in a Rayleigh faded environment.

Also shown in Table 4.3, the 16 QAM synchronous system shows the worst performance in the situation where omni-directional antenna is employed because of the high SINR requirement, which increases both the inter-cell and intra-cell interference. When 60° directional antenna is used, the 16 QAM system outperforms the other two systems. This is because the dominated interference is the intra-cell interference, and the synchronous system outperforms the asynchronous system in this situation. In addition, as mentioned above, the QPSK system has a capacity limit of 128 users/sector. Thus, for a 16 QAM system with a higher capacity limit, it can accommodate more users and performs better than the QPSK system. When large number of users is desired, trellis coded modulation is a better choice than 16 QAM as it has the same capacity limit of 256 users but performs better than 16 QAM in all situations; from Table 4.4, we find that the capacity of a system using TCM is

In conclusion, the synchronous system still outperforms the asynchronous system even in the worst situation shown in Table 4.3 (128 vs. 108). Also it is worth to note that the SINR measured at the base station is the signal to total noise and interference ratio. Thus, by employing synchronous transmission, the system is able to use less power for the same required SINR.

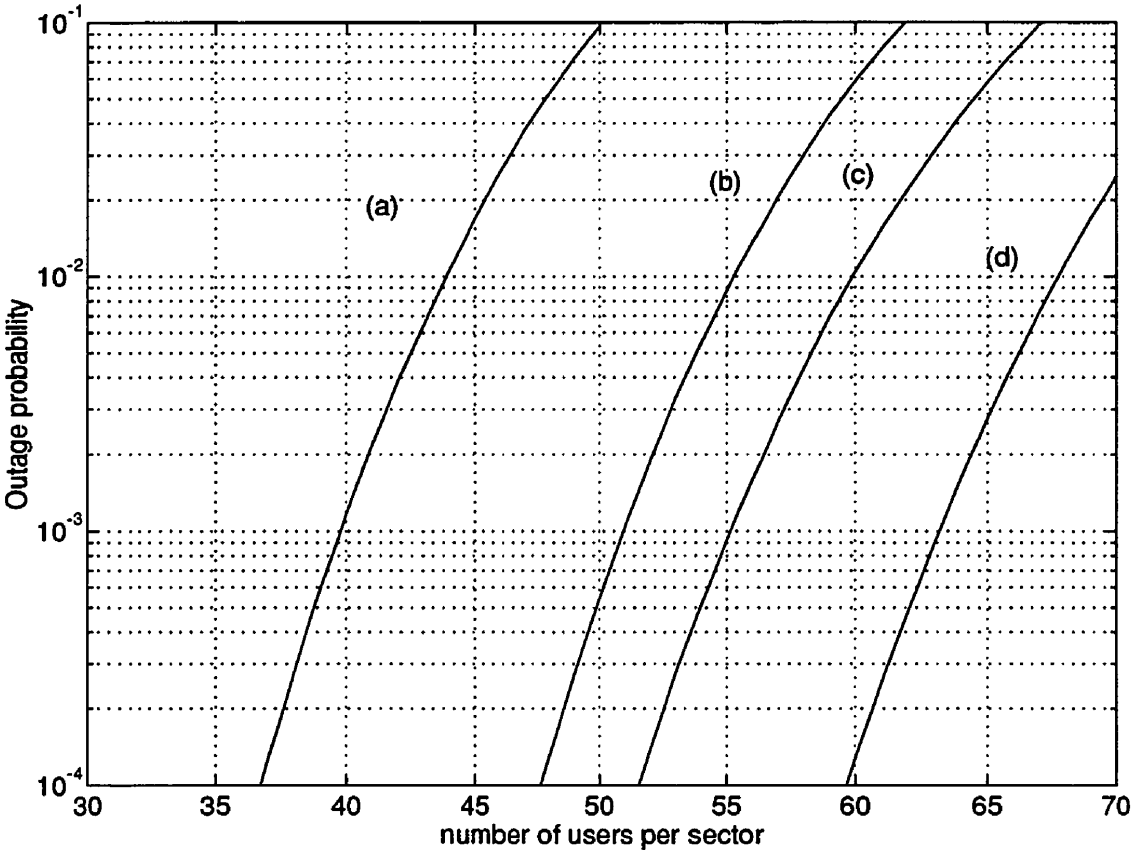

Figure 4.3: Outage probability versus the number of users per sector in a non-orthogonal system for (a) Rayleigh fading with one receive antenna, (b) Rician fading with K =10 and one receive antenna, (c) Rayleigh fading with selective receive antenna diversity (2 antennas), (d) no fading with one receive antenna.

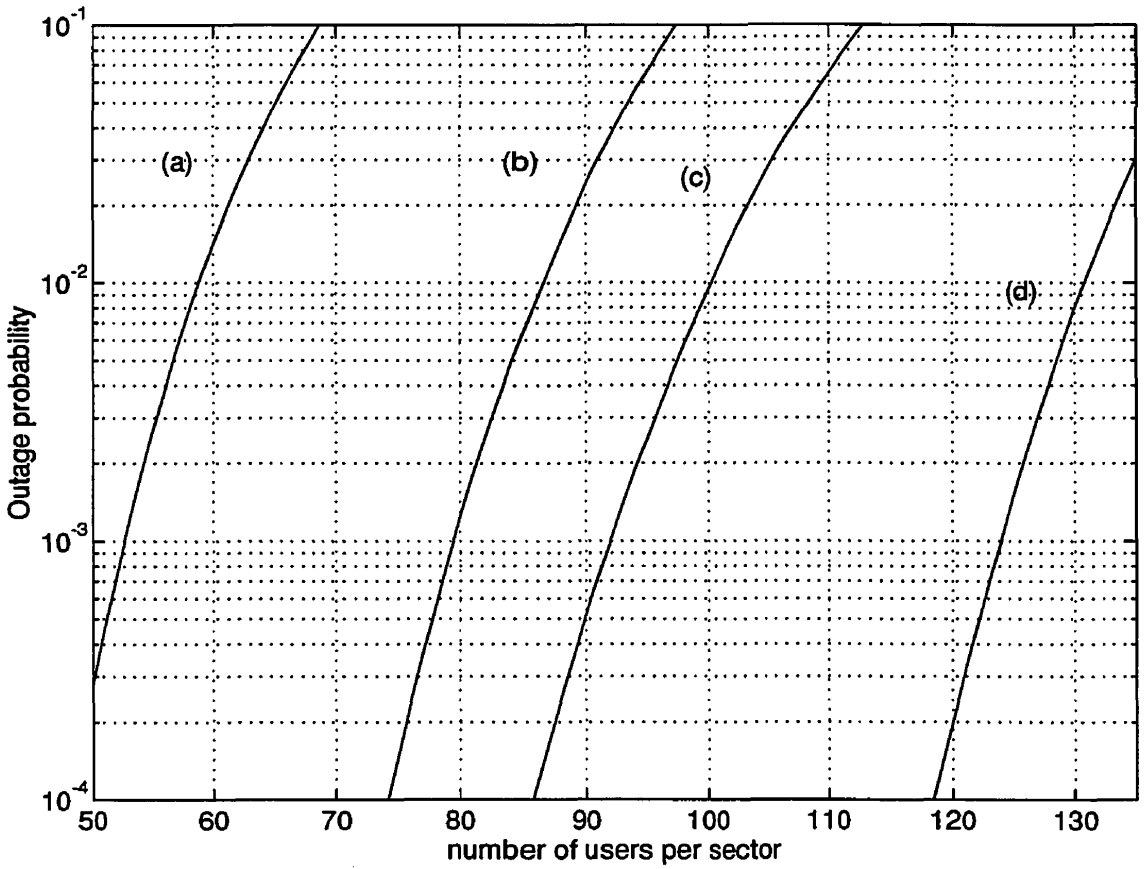

Figure 4.4: Outage probability versus the number of users per sector in a orthogonal system for (a) Rayleigh fading with one receive antenna, (b) Rician fading with K =10 and one receive antenna, (c) Rayleigh fading with selective receive antenna diversity (2 antennas), (d) no fading with one receive antenna.

K	No. of antenna	Antenna beam width	Synchronous /Asynchronous	Capacity
0	1	omni-directional	async	43
			sync (QPSK)	59
			sync (16QAM)	26
		120°	async	83
			sync (QPSK)	128†
			sync (16QAM)	100
		60°	async	95
			sync (QPSK)	128†
			sync (16QAM)	165
	2	omni-directional	async	61
			sync (QPSK)	87
			sync (16QAM)	46
		120°	async	93
			sync (QPSK)	128†
			sync (16QAM)	153
		60°	async	102
			sync (QPSK)	128†
			sync (16QAM)	231
10	1	omni-directional	asyn	55
			sync (QPSK)	100
			sync (16QAM)	40
		120°	async	90
			sync (QPSK)	128†
			sync (16QAM)	138
		60°	async	100
			sync (QPSK)	128†
			sync (16QAM)	215
∞	1	omni-directional	async	67
			sync (QPSK)	128†
			sync (16QAM)	63
		120°	async	97
			sync (QPSK)	128†
			sync (16QAM)	190
		60°	async	104
			sync (QPSK)	128†
			sync (16QAM)	256

Table 4.3: Comparison of the capacities for WLL systems with synchronous (QPSK and 16 QAM) and asynchronous reverse link transmissions with different number of receive antennas, beam width, and different fading environments. † 128 users per sector is the hard limit on system capacity for a QPSK system with rate 1/2 convolutional code and processing gain of 128.

K	No. of antenna	Antenna beam width	Synchronous /Asynchronous	Capacity
0	1	omni-directional	sync (8PSK TCM)	39
		120°	sync (8PSK TCM)	145
		60°	sync (8PSK TCM)	338
	2	omni-directional	sync (8PSK TCM)	67
		120°	sync (8PSK TCM)	219
		60°	sync (8PSK TCM)	256†
10	1	omni-directional	sync (8PSK TCM)	58
		120°	sync (8PSK TCM)	197
		60°	sync (8PSK TCM)	256†
∞	1	omni-directional	sync (8PSK TCM)	89
		120°	sync (8PSK TCM)	256†
		60°	sync (8PSK TCM)	256†

Table 4.4: Comparison of the capacities for WLL systems with synchronous reverse link transmissions (8PSK TCM) with different number of receive antennas, beam width, and different fading environments. † 256 users per sector is the hard limit on system capacity for a 8PSK TCM system.

Chapter 5

Conclusion

5.1 Thesis Summary

The liberalization of telecommunications industry has caused a high competition among telephone companies. As a result, radio has been considered, in addition to the traditional copper wire, to provide basic telephone services with low cost. CDMA has been shown to have the potential for providing higher capacity in mobile cellular networks in comparison to FDMA and TDMA [30]. It is believed that the advantages of using CDMA apply to the WLL system as well. Further capacity gain can be realized if we apply more sophisticated techniques to reduce the multiple access interference.

In Chapter 2, we find that the 1/2 chip quasi-synchronous system outperforms the conventional asynchronous system by 10 dB at $BER = 10^{-2}$ in a single cell system due to the reduction of the intra-cell interference. We also find that the coherent synchronization system performs 2.5 times faster than the non-coherent system. When the system is loaded with 64 users, the synchronization time is three times longer compared to a single user system due to the higher level of interference. The effect of MAI is alleviated by allowing higher transmitter power during the synchronization process. By allowing 3 dB higher in transmitter power, the synchronization time is reduced by one half. Also, it is shown that at the SINR of interest, the reverse link synchronization time is less than 100 ms and comparing to a typical call of 3-20 min [20], the cost of synchronizing the reverse link is insignificant.

QPSK scheme which doubles the spreading factor as compared to the IS-95 QPSK modulation scheme. Higher constellation modulation such as 16 QAM can further increase the spreading factor but the SINR required to achieve the same quality of service increases in a higher rate. Performance of best rate 1/2 and 1/4 convolutional code with constraint length of 9 is evaluated with different modulation schemes. For QPSK modulation, the minimum required SINR for achieving frame error rate less than 0.01 is equal to 2.5 and 3 dB, respectively. A 16 QAM system requires 5.7 dB to achieve the same frame error performance. For 8 PSK TCM, the required SINR is 3.9 dB.

In Chapter 4, we carried out a simulation to examine the overall capacity for the reverse link of a DS/CDMA WLL system. The result suggests that the use of receiver antenna diversity is not only essential for providing adequate coverage, it also increases the system capacity by reducing the variation of the fading amplitude; in a Rayleigh fading environment, the use of receiver antenna diversity increases the coverage by 28%. The simulation result also demonstrates the importance of LOS communication for the local loop system; system operates in a line of sight environment has capacity two times higher than the system operates in a non-LOS environment. The use of directional antenna has a great impact on the system capacity as we predicted; from the simulation result, the number of allowable users increases by 1.5 to 3 for every 10 degree decrease in antenna beam width. A synchronous system that employs high efficiency QPSK modulation and orthogonal spreading codes outperforms the asynchronous system in all situations; the performance gain ranges from 37% to 100% depending on the environment of operation and the techniques employed. Finally, synchronous system using 16 QAM gives the worst performance when omni-directional antenna is employed due to the higher power requirement. In the situation where a 60° directional antenna is used, the 16 QAM system, which has a higher capacity limit, has advantage over the QPSK system. It is also shown that if large number of users is desired, trellis coded modulation should be used as it has the same capacity limit but lower SINR requirement when compared with the 16 QAM system. In general, the high spectral efficiency QPSK system is preferred as it has high capacity and consumes the least power.

Some potential future research topics related to the work in this thesis are given below.

5.2.1 Other Applications of the WLL Systems

In this thesis, the WLL system is assumed to provide telephone services only. The frequency bands for the local loop service and the system bandwidth used in our analysis of the system performance follow exactly the IS-95 standard. As the WLL system is also currently considered for providing wireless multimedia data services; for example, the local multipoint communication system (LMCS), which is located at 25-28 GHz, is expected to provide services such as voice communications, digital TV broadcasting, and Internet access. The channel characteristics of LMCS are much different than that for the 900 MHz frequency bands as signals transmitted at frequencies of 25-28 GHz experience higher attenuation in propagation. The transmission in these frequency bands is also very sensitive to channel variation [11]; for example, the effect of rain and foliage attenuation can no longer be ignored as we did in our analysis. Thus, it is interesting to find out the performance of the synchronization system and the overall system capacity for such application with different channel characteristics.

5.2.2 Capacity of the WLL System with System Imperfections

In our design of the reverse link synchronization system and the analysis of system performance, numerous assumptions were made such as perfect power control, perfect carrier phase tracking, ideal antenna patterns (infinite attenuation outside main lobe) etc. It is shown that the capacity of a CDMA system may be significantly reduced under nonideal conditions [28]. Also, if trellis coded modulation is to be used in our system, the sensitivity to phase error should also be considered [22]. Thus, evaluating the capacity of the WLL system with the above system imperfections is another potential future work.

Appendix A

Markov Acquisition Model

The overall performance of the reverse link synchronization system is determined by the false alarm and detection probabilities. The false alarm occurs if a code phase is erroneously chosen as the correct code phase by the synchronization system. On the other hand, detection is achieved if the system can correctly find the code phase position. A more meaningful system characteristic is the mean synchronization time. The derivation of mean acquisition time (or mean synchronization system for our system) was thoroughly studied in [16] and a Markov acquisition model was developed. The mathematical detail is given in the rest of this section.

Due to the way in which the decision variable is processed, the acquisition process can be modeled as a Markov chain. If the detector output exceeds a preset threshold a hit is declared, and the system enters the tracking mode with single-dwell schemes. If the hit is corresponded to the correct phase, then the search process ends. However, if the hit is a false alarm, then the tracking loop detects the incorrect phase after certain time, and the system moves back to the acquisition mode. The time required for the system to detect a false alarm and then restart the acquisition process is called a penalty time. In a multiple-dwell schemes, a verification mode is added to avoid the cost of false alarm which results in long penalty time. Therefore, in the case of multiple-dwell schemes, a false alarm occurs if the incorrect code phase is erroneously confirmed by the verification algorithm. Thus, each code phase in the uncertainty region can be regarded as a state of the Markov chain. The code phase offset greater than a chip period is under hypothesis H_0. Otherwise, the code phase

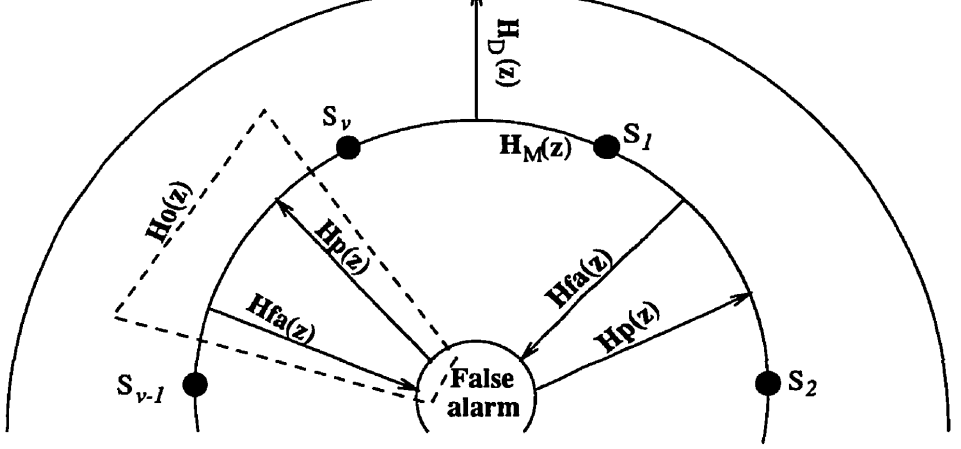

Figure A.1: Flow graph of serial search acquisition

position is under hypothesis H_1. Under hypothesis H_0, the system may go to either of two states. One is the false alarm state, resulting from an erroneous decision; the other state corresponds to the next code phase position. Under hypothesis H_1, the system advances to the detection state, if the correct code phase is detected by the acquisition algorithm; otherwise, a miss occurs and the next code phase position is examined.

For a system with uncertainty of v cells, $v+2$ states are required to model the process. Of the total of $v+2$ states, $v-1$ correspond to the code phase positions under hypothesis H_0, while one state corresponds to hypothesis H_1. The two remaining states are the *correct-acquisition* (ACQ) and *false-alarm* (FA) states. A segment of signal flow graph for serial search acquisition is shown in Figure A.1. Entry into the search process can occur at any one of the v starts, according to some priori distribution $(p_j, j = 1, 2, \cdots, v)$ which reflects the designer's confidence about the initial relative position of the codes. Uniform distribution $(p_j = \frac{1}{v}; j = 1, 2, \cdots, v)$ and worst-case location $(p_1 = 1, p_j = 0; j \neq 1)$ will result as special cases.

Let $p_{ij}(n)$ indicate the probability that the Markov process will move from state i to state j in n steps and let z indicate the unit-delay operator. If the unit delay specifically corresponds to τ seconds, z is replaced by z^τ in the following. The state

branch from i to j in the Markovian diagram is assigned a gain equal to $p_{ij}z$, where $p_{ij} = p_{ij}(1)$ is the one-step transition probability and z represents the unit delay associated with that transition [31]. Furthermore, we define the generating function

$$P_{ij}(z) = \sum_{n=0}^{\infty} p_{ij}(n)z^n \tag{A.1}$$

P_{ij} represents the transfer function from state i to state j of the flow graph. $P_{ij}(z)$ is useful because it contains statistical information about the Markovian process, and it can be derived through flow graph reduction methods.

In order to model the acquisition process as flow graph, we first assign gains $H(z)$ to the different branches of our model in Figure A.1 as follows: $H_D(z)$ is the gain of the branch leading from node H_1 (vth node) to the node ACQ; $H_M(z)$ is the gain of the branch connecting H_1 with state 1 and $H_0(z)$ is the gain of the branch connecting any other two successive states $(i, i+1); i = 1, \cdots, v-1$. Moreover, the system can move between any two successive states $(i, i+1)$ with $i \neq v$ either without false alarm (associated gain $H_{NFA}(z)$) or by first reaching the FA state (branch gain $H_{FA}(z)$), then pass from FA to state $i+1$ (associated branch gain $H_p(z)$) so that

$$H_0(z) = H_{NFA}(z) + H_{FA}(z)H_P(z). \tag{A.2}$$

The gains described above include all possible paths by which the process can move along the branch associated with that gain. So, $H_{NFA}(z)$ models all paths between successive H_0 states (such as partial false alarm) which do not lead to the false tracking-loop initiation; the latter path is modeled by $H_{FA}(z)$. $H_D(z)$ and $H_M(z)$ include all paths leading to successful acquisition or miss, respectively. From the flow graph in Figure A.1, we want the generating function

$$P_{ACQ}(z) = \sum_{i=1}^{v} p_i P_{i,ACQ}(z) \tag{A.3}$$

where p_i is the probability that the code search starts from the ith state. Taking the

structure of Figure A.1 into account,

$$P_{i,ACQ}(z) = \frac{H_D(z)H_0^{v-i}(z)}{1 - H_M(z)H_0^{v-1}(z)}. \tag{A.4}$$

Thus, for the case of arbitrary p_i

$$P_{ACQ}(z) = \frac{H_D(z)}{1 - H_M(z)H_0^{v-1}(z)} \sum_{i=1}^{v} p_i H_0^{v-i}(z). \tag{A.5}$$

For the case of uniform distribution, the generating function reduces to the following:

$$P_{ACQ}(z) = \frac{1}{v} \frac{H_D(z)(1 - H_0^v(z))}{(1 - H_M(z)H_0^{v-1}(z))(1 - H_0(z))}, \quad \text{uniform case} \tag{A.6}$$

From [32],[33], the mean and variance of the acquisition time can be expressed as

$$E(T_{acq}) = \frac{dP_{ACQ}(z)}{dz}|_{z=1} \tag{A.7}$$

$$\sigma^2_{T_{acq}} = \left[\frac{d^2P_{ACQ}(z)}{dz^2} + \frac{dP_{ACQ}(z)}{dz} - \left(\frac{dP_{ACQ}(z)}{dz}\right)^2\right]_{z=1} \tag{A.8}$$

For a scheme with non-absorbing false alarm state, which is common in practical situations, the mean acquisition times for uniform distributions are given by [16, 17]

$$E(T_{acq}) = \frac{1}{H_D(1)} \left[H'_D(1) + H'_M(1) + (v-1)H'_0(1)\left(1 - \frac{H_D(1)}{2}\right)\right], \quad \text{uniform case} \tag{A.9}$$

References

[1] W. C. Y. Lee, "Overview of Cellular CDMA," *IEEE Trans. Veh. Techno.*, vol. 40, pp. 291–302, May 1991.

[2] R. L. Pickholtz, L. B. Milstein, and D. L. Schilling, "Spread Spectrum for Mobile Communications," *IEEE Transactions on Vehicular Technology*, vol. 40, pp. 313–321, May 1991.

[3] Q. Chen, *Multi-Carrier DS-CDMA for Mobile Radio Systems.* PhD thesis, Electrical and Computing Department, University of Toronto, 1996.

[4] R. Price and P. Green, "A Communication Technique for Multipath Channels," *Proc. IRE*, pp. 555–570, March 1958.

[5] TIA-EIA-IS-95, *Mobile Station-Base Station Standard for Dual-Mode Wideband Spread Spectrum Cellular System*, JULY 1993.

[6] S. W. Golomb, *Shift Register Sequences.* San Franciso, CA: Holden Day, 1967.

[7] A. J. Viterbi, *Principles of Spread Spectrum Communication.* Addison-Wesley, 1995.

[8] S. H. Jamali and T. Le-Ngoc, *Coded Modulation Techniques for Fading Channels.* Kluwer Acadamic, 1984.

[9] H. Suzuki, "A Statistical Model for Urban Radio Propagation," *IEEE Transactions on Communication*, vol. COM-25, pp. 673–680, July 1977.

[10] W. C. Y. Lee, *Mobile Cellular Telecommunications: Analog and Digital Systems.* McGraw-Hill, Inc., 2 ed., 1995.

tions. Artech House, 1996.

[12] V. DaSilva, "Performance of Orthogonal CDMA Signals for Quasi-Synchronous Communication Systems," Master's thesis, Electrical and Computing Department, University of Toronto, 1993.

[13] S. G. Glisic, "Automatic Decision Threshold Level Control in Direct-sequence Spread Spectrum Systems Based on Matched Filtering," *IEEE Transactions on Communications*, vol. 36, pp. 519–527, APRIL 1988.

[14] Z.-L. Shi and P. F. Driessen, "Automatic Threshold Control for Acquisition in Spread Spectrum Packet Radio Communication," *Proceedings of Intl. Conference on Communications*, pp. 478–482, MAY 1993.

[15] A. C. K. Soong and W. A. Krzymien, "Performance of a reference symbol assisted multistage successive interference cancellation receiver in a multi-cell CDMA wireless system," *IEEE Global Telecommunications Conference*, pp. 152–156, 1995.

[16] A. Polydoros and C. L. Weber, "A Unified Approach to Serial Search Spread-Spectrum code Acquisition - Part II: A Matched-Filter Receiver," *IEEE Transactions on Communications*, vol. COM-32, pp. 550–560, MAY 1984.

[17] M. H. Zarrabizadeh, *Differentially Coherent Synchronization Schemes for Direct Sequence Spread Spectrum Communication Systems.* PhD thesis, Electrical and Computing Department, University of Toronto, 1995.

[18] V. DaSilva and E. S. Sousa, "Multicarrier orthogonal CDMA signals for quasi-synchronous communication Systems," *IEEE Journal on Selected Areas in Communications*, vol. 12, pp. 842–852, 1994.

[19] J. Sau, "Non-orthogonal Forward Link for Future CDMA Cellular Systems," Master's thesis, Electrical and Computing Department, University of Toronto, 1996.

dio telephone systems," *IEEE Transactions on Communications*, vol. COM-30, pp. 1905–1909, AUGUST 1981.

[21] J. G. Proakis, *Digital Communications.* McGraw-Hill, 3 ed., 1995.

[22] E. Biglieri, D. Divsalar, *et al.*, *Introduction to Trellis-Coded Modulation with Applications* . Macmillan, 1990.

[23] G. Ungerboeck, "Trellis-Coded Modulation with Redundant Signal Sets Part 1:Introduction," *IEEE Communications Magazine*, vol. 25, pp. 5–11, February 1987.

[24] G. Ungerboeck, "Trellis-Coded Modulation with Redundant signal Sets Part 2: State of the Art," *IEEE Communications Magazine*, vol. 25, pp. 12–21, February 1987.

[25] G. Ungerboeck, "Channel Coding with Multilevel/Phase Signals," *IEEE Transactions on Information Theory*, vol. IT-28, pp. 55–67, January 1982.

[26] S. Lin and D. J. Costello, *Error Control Coding: Fundamentals and Applications.* Prentice Hall, 1983.

[27] A. Jalali and P. Mermelstein, "Effects of Diversity, Power Control, and Bandwidth on the Capacity of Microcellular CDMA Systems," *IEEE Journal on Selected Areas in Communications*, vol. 12, pp. 952–961, JUNE 1994.

[28] P. Newson and M. R. Heath, "The Capacity of a Spread Spectrum CDMA System for Cellular Mobile Radio with Consideration of System Imperfections," *IEEE Journal on Selected areas in Communications*, vol. 12, pp. 673–683, MAY 1994.

[29] K. S. Gilhousen, I. M. Jacobs, *et al.*, "On the Capacity of a Cellular CDMA System," *IEEE Transactions on Vehicular Technology*, vol. 40, pp. 303–312, MAY 1991.

[30] P. Jung, P. W. baier, and A. Steil, "Advantages of CDMA and Spread Spectrum Techniques over FDMA and TDMA in cellular Mobile Radio Applications," *IEEE Transactions on Vehicular Technology*, vol. 42, pp. 357–363, August 1993.

cuit Theory, vol. CT-3, pp. 257–266, Dec 1956.

[32] P. M. Hopkins, "A unified analysis of pseudo-noise synchronization by envelop correlation," *IEEE Trans. Commun.*, vol. COM-25, pp. 770–778, Aug 1977.

[33] W. H. Huggins, "Signal Flow Graphs and Random Signals," *Proceeding of IRE*, pp. 74–86, Jan 1957.

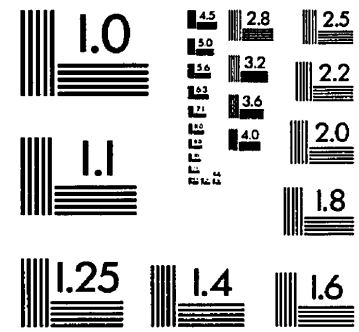

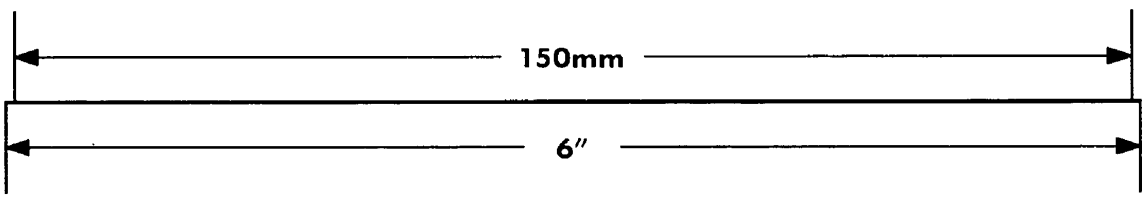

APPLIED IMAGE, Inc
1653 East Main Street
Rochester, NY 14609 USA
Phone: 716/482-0300
Fax: 716/288-5989